# ERK regulates microglial immune responses in Alzheimer's disease

### **Authors**

Michael J Chen,\*1 Supriya Ramesha,\*1 Laura D. Weinstock,3,4 Tianwen Gao,1 Lingyan Ping,2 Hailian Xiao,1 Eric B Dammer,2 Duc D Duong,2 Allan I Levey,1 James J Lah,1 Nicholas T Seyfried,2 Levi B. Wood,\*3,4,5 Srikant Rangaraju\*1

#### Authors:

Srikant Rangaraju, Email: Srikant.rangaraju@emory.edu Phone: 1-404-727-0633

Levi Wood, Email: levi.wood@me.gatech.edu Phone: 1-617-388-9950

Michael J Chen, Email: <a href="michael.jiabo.chen@emory.edu">michael.jiabo.chen@emory.edu</a>
Supriya Ramesha, Email: <a href="michael.juanuning.supriya.ramesha@emory.edu">supriya.ramesha@emory.edu</a>
Laura D Weinstock, Email: <a href="michael.jweinstock3@gatech.edu">jweinstock3@gatech.edu</a>
Tianwen Gao, Email: <a href="michael.juanuning.gao@emory.edu">jianwen.gao@emory.edu</a>
Linyang Ping, Email: <a href="michael.juanuning.gaomory.edu">jianwen.gao@emory.edu</a>
Hailian Xiao, Email: <a href="michael.jiabo.chen@emory.edu">hiing.gaomory.edu</a>
Hailian Xiao, Email: <a href="michael.jiabo.chen@emory.edu">hiing.gao@emory.edu</a>

Hailian Xiao, Email: <a href="mailto:hxiao6@emory.edu">hxiao6@emory.edu</a>
Eric B Dammer, Email: <a href="mailto:edammer@emory.edu">edammer@emory.edu</a>
Duc D Duong, Email: <a href="mailto:dduong@emory.edu">dduong@emory.edu</a>
Allan I Levey, Email: <a href="mailto:jlah@emory.edu">jlah@emory.edu</a>
James J Lah, Email: <a href="mailto:jlah@emory.edu">jlah@emory.edu</a>

Nicholas T Seyfried, Email: nseyfri@emory.edu

Word count: Abstract 238 Total: 10,956

Figures: 8 Tables: 1

Supplementary figures: 7 Supplementary tables: 10

<sup>\*</sup>Equal contribution as first authors

<sup>#</sup>Equal contribution as senior/corresponding authors

<sup>^</sup>Lead contact

<sup>&</sup>lt;sup>1</sup>Department of Neurology, Emory University, Atlanta GA 30322 USA

<sup>&</sup>lt;sup>2</sup>Department of Biochemistry, Emory University, Atlanta GA 30322 USA

<sup>&</sup>lt;sup>3</sup>Parker H. Petit Institute for Bioengineering & Bioscience, Georgia Institute of Technology, Atlanta, GA 30332

<sup>&</sup>lt;sup>4</sup>The Wallace H. Coulter Department of Biomedical Engineering, Georgia Institute of Technology, Atlanta, GA 30332

<sup>&</sup>lt;sup>5</sup>George W. Woodruff School of Mechanical Engineering, Georgia Institute of Technology, Atlanta, GA 30332

SIGNIFICANCE STATEMENT

We report that ERK activation is characteristic of activated microglia in an Aβ mouse model of

Alzheimer's disease pathology. Inhibition of ERK activation in primary microglia dampened

IFNγ-induced pro-inflammatory gene expression and suppressed neuronal phagocytic activity,

suggesting that ERK activity in microglia may regulate detrimental pro-inflammatory responses.

Analyses of global and phospho-proteomic data from post-mortem human brain indicate increased

ERK activation in human Alzheimer's disease. Our integrated analyses provide novel insights into

ERK activation in microglia and support a critical role for ERK signaling in Alzheimer's disease

pathogenesis.

Keywords: Microglia, ERK, Alzheimer's disease, proteomics, neuroinflammation,

RRID:SCR\_002865, RRID:IMSR\_JAX:000664, RRID:MMRRC\_034840-JAX,

RRID:SCR\_002798, RRID:AB\_394489, RRID:AB\_396772, RRID:AB\_331646,

RRID:AB\_354872, RRID:SCR\_003420, RRID:SCR\_017386, RRID:CVCL\_0470

**ABBREVIATIONS** 

AD: Alzheimer's disease

ERK: extracellular signal-regulated kinase

MAPK: mitogen-activated protein kinase

DAM: disease-associated microglia

Aβ: amyloid beta

IFNγ: interferon gamma

LPS: lipopolysaccharide

TMT: tandem mass tag

2

GO: Gene ontology

KEGG: Kyoto Encyclopedia of Genes and Genomes

PANTHER: Protein ANalysis THrough Evolutionary Relationships

JNK: c-Jun N-terminal kinase

NFκB: Nuclear factor kappa-light-chain-enhancer of activated B cells

RTK: Receptor tyrosine kinase

5xFAD: Refers to Tg(APPSwFlLon,PSEN1\*M146L\*L286V)6799Vas/Mmjax strain on

C57BL6/J background

MAGMA: Multi-marker Analysis of GenoMic Annotation

### **ABSTRACT**

The importance of MAPK pathway signaling in regulating microglia-mediated neuroinflammation in Alzheimer's Disease remains unclear. We examined the role of MAPK signaling in microglia using a pre-clinical model of Alzheimer's disease pathology and quantitative proteomics studies of post-mortem human brains. In multiplex immunoassay analyses of MAPK phosphoproteins in acutely-isolated microglia and brain tissue from 5xFAD mice, we found phosphorylated ERK was the most strongly upregulated phospho-protein within the MAPK pathway in acutely-isolated microglia but not whole brain tissue from 5xFAD mice. The importance of ERK signaling in primary microglia cultures was next investigated using transcriptomic profiling and functional assays of amyloid β and neuronal phagocytosis, which confirmed that ERK is a critical regulator of IFNy-mediated pro-inflammatory activation of microglia, although it was also partly important for constitutive microglial functions. Phospho-ERK was an upstream regulator of diseaseassociated microglia (DAM) gene expression (Trem2, Tyrobp), as well as several human Alzheimer's disease risk genes (Bin1, Cd33, Trem2, Cnn2), indicative of the importance of microglial ERK signaling in AD pathology. Quantitative proteomic analyses of post-mortem human brain showed that ERK1 and ERK2 were the only MAPK proteins with increased protein expression and positive associations with neuropathological grade. In a human brain phosphoproteomic study, we found evidence for increased flux through the ERK signaling pathway in AD. Overall, our analyses strongly suggest that ERK phosphorylation, particularly in microglia in mouse models, is a regulator of pro-inflammatory immune responses in Alzheimer's disease pathogenesis.

#### INTRODUCTION

Microglia, the primary immune cells of the brain, are the key enactors of neuroinflammation in Alzheimer's disease (AD) (Hickman, Izzy, Sen, Morsett, & El Khoury, 2018; Lambert et al., 2013), orchestrating both beneficial and detrimental mechanisms in context-dependent manners (Bachiller et al., 2018; Dubbelaar, Kracht, Eggen, & Boddeke, 2018; Tay et al., 2017). Detrimental consequences of microglia are mediated by pro-inflammatory mechanisms, including reactive oxygen species, cytokines (IL1β, TNFα, IL6), phagocytosis of synapses and dendrites, and impaired phagocytic clearance of pathological proteins. Microglial can also promote pathogenesis via indirect mechanisms involving astrocytes or oligodendroglia, which then impact neuronal health and survival (Block, Zecca, & Hong, 2007; Geraghty et al., 2019; Hagemeyer et al., 2017; Liddelow et al., 2017; Sellgren et al., 2019). Defining critical regulators of homeostatic, disease-associated, and pro-inflammatory microglial responses in AD (Srikant Rangaraju et al., 2018) can lead to neuro-immunomodulatory therapies that selectively inhibit pro-inflammatory responses without impacting homeostatic functions.

Distinct microglial immunological profiles are likely to be determined by upstream signaling events that are engaged by cytokines, pathological proteins, and oxidative stress in the setting of neurodegeneration. Signaling pathways, such as the mitogen activated protein kinase (MAPK) family of proteins, are engaged very early in immune cells (Cargnello & Roux, 2011). MAPKs includes over 60 proteins broadly categorized into three families, namely the ERK, JNK, and p38 cascades (Yates et al., 2017), which are initiated via activation of a cell surface receptor, triggering serial phosphorylation events by serine/threonine protein kinases, ultimately activating or suppressing transcription factors (TFs) (Arkun & Yasemi, 2018; Santos, Verveer, & Bastiaens, 2007). ERK signaling is initiated by receptor tyrosine kinases (RTKs) that are typically receptors for growth factors. JNK signaling, which is activated by cellular stress, is associated with increased

formation of amyloid  $\beta$  (A $\beta$ ) plaques and neurofibrillary tangles, as well as neuron apoptosis in AD (Yarza, Vela, Solas, & Ramirez, 2016). p38 is activated by inflammatory stimuli and cytokines (Lee & Kim, 2017). There is also significant cross talk between these three cascades, particularly JNK and p38 (Zhang & Liu, 2002). While these signaling events are typically transient and often necessary for homeostasis, constitutive functions, and proliferation, sustained activation may lead to dysfunction and chronic inflammatory activation in microglia (Kim, Smith, & Van Eldik, 2004). However, the importance of MAPK signaling in regulating microglia-mediated neuroinflammation in AD remains unclear.

We investigate the role of MAPK signaling using phospho-protein signaling studies of acutely-isolated microglia and whole-brain tissues from 5xFAD mice to reveal microglia-specific ERK activation signaling in AD pathology. In neuroinflammatory transcriptomic profiling of primary mouse microglia, we show that ERK signaling is a critical regulator of pro-inflammatory microglial activation in response to interferon  $\gamma$  (IFN $\gamma$ ), in addition to being an upstream regulator of several disease-associated microglial genes and genetic risk factors for late-onset AD. We further interrogated human post-mortem mass-spectrometry data from control and AD brains and provide evidence for increased ERK activation. Our integrated approach synthesizes data from mouse microglia and whole post-mortem human brains and provides novel insights into the role of ERK signaling in AD.

### MATERIALS AND METHODS

**Animals:** All mouse experiments were performed in accordance with policies and procedures described in the Guide for the Care and Use of Laboratory Animals of the National Institutes of Health and were approved by the Institutional Animal Care and Use Committee at Emory

University. C57BL/6J (RRID:IMSR\_JAX:000664) and 5xFAD mice (RRID:MMRRC\_034840-JAX) were bred and housed in a 12/12 h light/dark cycle.

**Mouse microglia isolation and** *in-vitro* **studies**: Adult microglia were isolated from the brains of wild-type and age-matched 5xFAD mice (age 6-7 mo, n=7/group including 3 males and 4 females) using Percoll density centrifugation (35%/70%), followed by enrichment of CD11b<sup>+</sup> microglia by magnetic-activated cell sorting (Miltenyi Biotec) and frozen on dry ice for Luminex phosphoprotein signaling studies (Srikant Rangaraju et al., 2018).

Primary microglia cultures were prepared from P0-3 post-natal mouse brains as previously described (Gao et al., 2019). Briefly, brain tissue was harvested from C57BL/6J mice (P0 to P3) and digested with Trypsin for 15 min. Trypsinization was halted by the addition of Dulbecco's Modified Eagle Medium: Nutrient Mixture F-12 (DMEM-F12) supplemented with 10% fetal bovine serum (FBS) and 1% penicillin-streptomycin-glutamine. Once filtered using a 40 μm nylon mesh strainer, the resulting cell suspension was positively selected for CD11b<sup>+</sup> cells using mini-MACS columns. The cells, almost entirely consisting of microglia, were seeded into poly-Llysine-coated wells and cultured in a humidified CO<sub>2</sub> incubator at 37°C. Following 24 h of incubation, half of the medium was replaced with fresh medium and 1μM SCH772984, a selective small molecule inhibitor of ERK 1/2 (IC<sub>50</sub> for ERK1: 4nM, IC<sub>50</sub> for ERK2: 1 nM) was added to the culture (Morris et al., 2013). After 1 h of pre-incubation, cells were stimulated with 1 ng/mL IFNγ (Sigma) and then incubated for 24 h, after which cells were trypsinized and harvested for downstream analyses.

Luminex phospho-protein analyses of acutely-isolated microglia from mouse brain: Collected microglia were lysed in Bio-Plex lysis buffer (Bio-Rad) with the addition of 1 Complete Mini (Roche) protease inhibitor per 5mL of buffer. Cells were lysed for 10 min on an end-overend rotator, then centrifuged at 13kRPM for 10 min with supernatant collected and stored at -80°C. Protein yield was measured using Pierce BCA Protein Assay kit (ThermoFisher Scientific) and 0.1μg of total protein from each sample was added to the Luminex assay. Phospho-signaling was quantified using the MAPK/SAPK Signaling 10-Plex Multiplex assay (Millipore Sigma, 48-660MAG). Phosphorylation sites for the MAPK/SAPK as follows: ATF2 (Thr71), ERK (Thr185/Tyr187), HSP27\* (Ser78), JNK (Thr183/Tyr185), c-Jun (Ser73), MEK1 (Ser222), MSK1 (Ser212), p38 (Thr180/Tyr182), p53\* (Ser15) and STAT1 (Tyr707). Analytes marked with an asterisk have not been reported to be mouse-reactive and were removed from the analysis. The assay was read out using a MAGPIX instrument (Luminex, Austin, TX, USA).

NanoString transcriptomic profiling of microglia and statistical analyses: NanoString transcriptomic profiling of mRNA isolated from primary mouse microglia was performed as previously published (Gao et al., 2019). Primary microglia were treated with the ERK inhibitor in the presence or absence of IFNγ. The cells were washed in 1x Diethyl pyrocarbonate-phosphate buffered saline and lysed in TRIzol (Invitrogen). RNA was extracted using the nCounter Low RNA Input Kit, and a quality control assessment was performed to determine concentration and integrity of RNA (RIN scores >8). 100 ng of RNA per sample was run using the nCounter Mouse Neuroinflammation Panel (770 genes) and gene expression data was imported into nSolver Analysis Software (Version 4.0, RRID:SCR\_003420). After background thresholding, genes for which >50% of samples exceeded this threshold (n=678) were analyzed. Expression levels were normalized to positive controls and then to 12 housekeeping genes and analyzed by ANOVA (two-tailed) and Tukey's post-hoc tests for groupwise differences. Differentially-expressed transcripts

(p < 0.05)included K-means (Morpheus: were clustering analysis (https://software.broadinstitute.org/morpheus, RRID:SCR 017386; Metric: one minus Pearson correlation with 1000 maxim iterations). We applied a combination of hierarchical clustering and K-means clustering approaches to identify the ideal number of clusters that best described groupwise differences and distinct expression patterns based on ERK inhibitor and IFNγ exposures. We first explored the data using hierarchical clustering analysis (one minus Pearson correlation metric, average linkage method) which revealed that at least 4, up to 6 distinct clusters of genes exist in the dataset. We then performed K-means clustering using a range of potential cluster solutions (range 2-8) and identified 5 as the optimal cluster size. Gene ontology (GO) enrichment analysis was performed on the resulting clusters using GO-Elite (version 1.2.5), to identify GO, KEGG pathway and Wikipathway terms enriched in lists of genes as compared to a reference list of genes (Zambon et al., 2012). We also used t-weighted stochastic neighbor embedding (t-SNE) to visualize clusters of genes in two dimensions and determine whether known homeostatic microglia and disease-associated-microglia (DAM) genes mapped to specific gene clusters identified in our dataset. We used existing reference transcriptomes and network analyses to obtain lists of homeostatic and DAM genes (Keren-Shaul et al., 2017) and lists of genes specific to modules of co-expressed microglial genes previously identified using network analysis (Srikant Rangaraju et al., 2018).

Flow cytometry studies: Flow cytometric assays of microglia viability, A $\beta$  phagocytosis, and microglia-mediated neuronal phagocytosis were performed using *in-vitro* primary mouse microglia. To assess the viability of microglia under the experimental conditions, primary microglia were treated with the ERK inhibitor and/or IFN $\gamma$  as above. After 24 h, the cells were

washed in PBS and trypsinized (15 min 37°C) and cells were washed and incubated with LIVE/DEAD indicator (30 min). After washing (2% normal horse serum and PBS), PE-Cy7 antimouse CD45 mAb was added (dark, 30 min), after which the cells were washed in PBS. Compensation, gating, live/dead exclusion and data analysis for flow cytometry were performed as published (Srikant Rangaraju et al., 2018).

The effect of ERK inhibition and inflammatory stimulation on microglial phagocytosis of fluorescent fibrillar amyloid- $\beta_{42}$  (fA $\beta$ 42) was determined by flow cytometry as previously described (Gao et al., 2019; S. Rangaraju, S. A. Raza, et al., 2018). Primary microglia treated with the ERK inhibitor and/or IFN $\gamma$  were incubated with 2 $\mu$ M of fA $\beta$ 42-488 for 1h (37°C) and then subsequently labeled with anti-CD45, and phagocytosis was assessed by observing the second peak of fluorescence which represents actin-dependent A $\beta$  phagocytosis (Srikant Rangaraju et al., 2018).

To measure microglia-mediated neuronal phagocytosis, we performed microglia-neuron co-culture studies using mouse N2a cells (RRID:CVCL\_0470) stably transduced to express GFP (Lenti-Ubc-GFP/FUGW, Addgene#14883) and primary p0-3 mouse microglia, and used flow cytometry to detect microglial uptake of GFP<sup>+</sup> neuronal material. GFP-N2a cells were washed twice with medium and allowed to grow to 70-80% confluence. 50,000 N2a cells were seeded into 12-well plates, and 24 h later, the medium was replaced with DMEM with 1% FBS and 10 μM retinoic acid to induce differentiation for 4 days (Namsi et al., 2018). Meanwhile, primary microglia were cultured in the presence or absence of IFNγ and treated with the ERK inhibitor (or DMSO control) as described above. After 4 days of N2a neuronal differentiation, fresh medium with 1% FBS replaced the differentiation medium, and 100,000 microglia were seeded into the differentiated N2a culture. Co-cultures were incubated for 24 h and then trypsinized for 2 min at

37°C for antibody staining. The cells were washed sequentially with 1% FBS and PBS and labelled with LIVE/DEAD indicator and anti-CD45 (PC-Cy7). Microglial phagocytosis of neuronal cells was assessed by determining GFP positivity in live microglia via flow cytometry with appropriate negative controls (microglia without neurons). Viability of CD45<sup>+</sup> microglia and N2a-GFP<sup>+</sup> cells were assessed.

Flow cytometry for phospho-ERK1/2 was performed in acutely-isolated brain mononuclear cells derived from wild-type and 5xFAD mice. The cells were labeled with fluorophore-conjugated mAbs against CD11b (APC-Cy7) and CD45 (PE-Cy7), then fixed with fixation buffer for 10 min at RT and then permeabilized with cold methanol (30 min, 4°C, dark) and blocked (Fc-block Biolegend Cat #553142) (30 min). Cells were incubated with primary anti-phospho-ERK1/2 (1:100) or anti-ERK (1:20) (30 min) followed by secondary antibody (Goat anti-rabbit-FITC, 1:500, 30min) followed by flow cytometry. Appropriate negative (unstained), secondary-alone and fluorescence-minus-one controls were performed for all experiments involving unconjugated primary antibodies. Single microglia that expressed CD11b and 5xFAD microglia.

Quantitative reverse transcriptase PCR (qRT-PCR): qRT-PCR was performed using RNA isolated from primary microglia (Gao et al., 2019) cultured in the conditions mirroring the NanoString studies. RNA was isolated from microglia, and RNA concentration and purity were determined using the NanoDrop 2000 spectrophotometer. cDNA was synthesized, and qRT-PCR was performed on the 7500 Fast Real-time PCR System (Applied Biosystems), TaqMan PCR master mix (Applied Biosystems), and gene-specific TaqMan probes (Applied

Biosystems) against Apoe (Mm01307193\_g1), Tnf (Mm01210732\_g1), Trem2 (Mm04209424\_g1), Tyrobp (Mm00449152\_m1), Spp1 (Mm00436767\_m1), and Gapdh (Mm99999915\_g1). All primer sets were run in duplicate and 3 biological replicates were performed per condition. Gene expression was normalized to the housekeeping gene, Gapdh, and relative gene expression was calculated using the 2-ΔΔCt method.

Human post-mortem brain quantitative proteomics data: Two existing post-mortem brain proteomic datasets were used for analyses. The first is a published dataset in which dorsolateral prefrontal cortex (age-matched non-disease controls, AD cases, Parkinson's disease and both AD and Parkinson's disease, n=10/group) were sampled for tandem mass tag mass spectrometry (TMT-MS) (L. Ping et al., 2018). The second dataset is a phospho-proteomics TMT-MS dataset of non-disease controls, asymptomatic AD cases and AD cases with dementia (n=6/group). Methodology used for phospho-peptide enrichment by immobilized metal-affinity chromatography (IMAC) and isobaric tandem mass tag mass spectrometry have been previously published (Dai et al., 2018; Dammer et al., 2015). Total protein (dataset 1) and phospho-peptide data (dataset 2) pertaining to MAPKs were used for analyses. Spearman's Rank correlation coefficient was calculated in SPSS to assess the relationship between MAPK1 and MAPK3 protein expression levels with BRAAK stage. The clinical and demographic data for these study cohorts are presented in Supplementary Table 1.

**Materials:** ERK1/2 inhibitor SCH772984 was obtained from Selleckchem (S7101). The following reagents were used for studies: CD45-PE-Cy7 Rat mAb (BD Biosciences, #552848, RRID:AB 394489), LIVE/DEAD Fixable Blue Stain (Invitrogen, L34961), CD11b-APC-Cy7 Rat

mAb (BD Biosciences, #557657, RRID:AB\_396772), phospho-ERK1/2 Rabbit pAb (Cell Signaling Technology, #9101S, RRID:AB\_331646) and ERK1/2 Rabbit pAb (R&D Systems, AF1576, RRID:AB 354872). Details about antibodies used are summarized in **Table 1**.

Statistical considerations: GraphPad Prism (Ver. 5, RRID:SCR 002798) and SPSS (Ver. 26, RRID:SCR 002865) were used to create graphs and for statistical analyses. Error bars in all bar graphs represent the standard deviation (SD). We determined sample size for Luminex studies of CD11b+ MACS-purified microglia (n=7-9/group) based on the following parameters: expected difference between means of 25%, a standard deviation of 15%, alpha level 5%, and power of 80%. We included male and female mice across all groups. All other experiments did not have a power calculation. For experiments with > 2 groups, one-way ANOVA was performed as previously described in R (Ver 4.0.2) (R Core Team, 2020; Seyfried et al., 2017) to detect differences across groups and post-hoc pairwise comparisons were performed using post-hoc Tukey's test (p<0.05 considered significant for all experiments). Clustering analyses for visualization of Nanostring performed Morpheus data were using (https://software.broadinstitute.org/morpheus) as described above.

## **RESULTS**

## Phosphorylated ERK and p38 MAPK are increased in microglia in 5xFAD mice.

MAPKs are comprised of three sub-families of signaling proteins, namely ERK, JNK, and p38 pathways (**Figure 1a**). To determine whether MAPK signaling is chronically upregulated in microglia in a mouse model of AD pathology, we acutely-isolated CD11b<sup>+</sup> brain myeloid cells from adult (6-7 mo old) wild-type and age/sex-matched 5xFAD mice that exhibit accelerated Aβ

pathology in the brain. CD11b<sup>+</sup> brain myeloid cells are comprised primarily (>95%) of microglia and a small proportion of CNS-infiltrating monocytes/macrophages with >95% viability (Srikant Rangaraju et al., 2018). We broadly interrogated phospho-signaling within MAPK pathways in microglia by assaying phosphorylation of 9 proteins within the three MAPK pathways (Figure 1b). We simultaneously quantified signaling within whole tissue samples obtained from the frontal cortex where Aβ pathology is abundant in 5xFAD mice. Compared to microglia isolated from WT mice, 5xFAD mouse microglia exhibited increased activation of ERK signaling, indicated by increased phospho-ERK1/2 (p-ERK1/2) (two-tailed independent sample t-test, t (13)=2.98, p=0.009) and trend towards increased levels of phospho-MEK1 (p-MEK1) (two-tailed independent sample t-test, t (13)=1.8, p=0.090), an upstream ERK activator. Increased p38 MAPK activation was also observed, indicated by higher phospho-p38 (p-p38 levels) in 5xFAD microglia (two-tailed independent sample t-test, t (13)=2.15, p=0.048) (Figure 1c). Unlike in microglia, we did not observe any differences in MAPK signaling in whole brain tissue (Supplementary Figure 1). These findings provide evidence for increased activation of MAPKs, particularly ERK1/2, in microglia in 5xFAD mice.

## MAPK Protein Expression is Unaltered in 5xFAD microglia.

To ascertain expression levels of MAPKs at the total protein level in mouse microglia, we assessed the relative abundance of total MAPK proteins (versus non-MAPK proteins) in recently published proteomic datasets obtained from purified mouse microglia, as well as BV2 mouse microglia (S. Rangaraju, E. B. Dammer, et al., 2018; S. Rangaraju, S. A. Raza, et al., 2018). In total, 60 genes/proteins have been classified as belonging to the family of MAPK cascades (Supplementary Table 2) (Yates et al., 2017). Of these, 17 MAPK proteins (total protein levels)

were identified in acutely-isolated CD11b<sup>+</sup> microglia from 6 mo old mice (pooled analysis of wildtype, 5xFAD, and systemic LPS-treated wild-type mice) (Figure 2a), while 10 MAPK proteins were identified in BV2 microglia (Figure 2b). Interestingly, relative abundances of ERK proteins were highest in both acutely-isolated mouse microglia (Figure 2a), as well as in BV2 microglia (Figure 2b) compared to other MAPKs. Compared to wild-type microglia, 5xFAD microglia showed lower total protein levels of RAF1 (F(2,6)=12.7, n=3, p= 0.007, post-hoc p=0.03) and MAP2K6 (F(2,6)=15.9, n=3, p=0.004, post-hoc p=0.033), while microglia isolated from LPStreated mice showed increased total levels of two ERK proteins, namely MAPK1 (F(2,6)=4.5, n=3, p=0.061, post-hoc p=0.080) and MAPK3 (F(2,6)=21.8, n=3, p=0.002, post-hoc p=0.006), and lower levels of TAOK1 (F(2, 6)=8.1, n=3, p=0.020, post-hoc p=0.033) and RAF1 (post-hoc p=0.009) (Figure 2c). While our Luminex studies showed alterations in levels of activated ERK phospho-proteins in 5xFAD microglia, proteomic studies show that total protein levels of ERK1 and ERK2 were not altered in 5xFAD microglia. Consistent with this, we performed flow cytometric studies of acutely-isolated brain myeloid cells (Figure 2d), confirming that intracellular p-ERK1/2 levels were increased in 5xFAD microglia as compared to wild-type microglia (two-tailed independent sample t-test, t (10)=3.16, p=0.010), whereas total ERK1/2 was equal between the groups (Figure 2d-e).

In summary, our findings demonstrate that MAPK signaling proteins belonging to the ERK cascade are highly abundant in microglia and that microglia in an AD mouse model exhibit upregulation of ERK phospho-signaling, supporting critical roles for ERK signaling in regulating neuroinflammation in AD.

In-vitro analysis reveals that ERK signaling is a critical regulator of pro-inflammatory microglial activation.

ERK signaling may be an important regulator of pro-inflammatory microglial activation (Gao et al., 2019). Based on our results showing increased ERK signaling in 5xFAD microglia and the relevance of ERK to human AD pathology, we next hypothesized that ERK is a key regulator of DAM gene expression, particularly pertaining to pro-inflammatory responses that can be detrimental in AD. We exposed mouse primary microglia to a selective ERK1/2 inhibitor (SCH772984,  $1\mu$ M) in the presence or absence of IFN $\gamma$  (1ng/mL) and performed viability studies and neuroinflammatory transcriptomic profiling (770 genes). For our in-vitro studies, we selected IFN $\gamma$  as a canonical immune stimulus to mirror pro-inflammatory activation of microglia and induce M1-like characteristics. IFN $\gamma$ , produced by glia and lymphocytes, is also known to regulate gene expression of several AD-related genes and regulates A $\beta$  and tau pathology in mouse models of AD pathology (Mastrangelo, Sudol, Narrow, & Bowers, 2009).

Overall, ERK inhibition minimally impacted cell health and viability under our experimental conditions (Supplementary Figure 2). Of the 770 genes in the NanoString panel, 678 were included in the final analysis (Supplementary Table 3), and ANOVA identified 465 genes with differential expression across all 4 groups (436 genes FDR adjusted p<0.05). K-means clustering of these differentially expressed genes revealed 4 main clusters of genes (Figure 3a, Supplementary Table 4). Cluster 1 consisted of genes negatively regulated by ERK under both unstimulated and IFNγ-stimulated conditions. Cluster 2-4 were all positively regulated by ERK signaling. Cluster 2 was suppressed by IFNγ, Cluster 3 was upregulated by IFNγ, and Cluster 4 was not affected by IFNγ. The most statistically significant and representative genes for each cluster are shown in Figure 3a. A smaller cluster of 17 genes, Cluster 5, contained genes

upregulated by IFNγ independent of ERK; in fact, several genes in this cluster align with existing literature as being positively regulated by IFNγ (e.g. Stat1 and Irf1) (Zhou, Zoller, Krieglstein, & Spittau, 2015). Despite being biologically meaningful, however, we did not draw attention to this cluster because it was not conserved across multiple runs of K-means analysis and confidence in this cluster is low given its small size.

To obtain a functional understanding of the clustered genes, we next performed GO enrichment analyses (GOElite) using all included genes in the neuroinflammation panel as the reference. Cluster 1 genes were enriched for neuronal/synaptic and glutamatergic transcripts with generally low abundance. Cluster 2 was enriched for genes involved in IGF1 receptor signaling, negative regulation of apoptosis, cell differentiation and energy metabolism, and integrin binding. Cluster 3 was enriched with genes involved in pro-inflammatory signaling and immune processes, cytokine activity, and TF activity in the nucleus. Cluster 4 was enriched with genes involved in DNA replication, cell division, cytokine secretion, ribosomal machinery, and purine metabolism (Figure 3b). Additional KEGG and Wikipathway enriched terms are shown in Supplementary **Table 5**. Since ERK signaling regulates TF activity, we used bioinformatics approaches (Metacore, Thompson Reuters) to identify TFs down-stream of ERK activation that are likely to regulate gene expression in Cluster 2, 3, and 4 genes (Supplementary Table 6). PU.1, c-Jun, Bcl-6, SP3, EGR1, and SP1 were top predicted TF regulators of Cluster 2 genes, consistent with known importance of PU.1, c-Jun, and SP1 in microglial development and survival and the enrichment of homeostatic genes within cluster 2 (Rustenhoven et al., 2018; Smith et al., 2013). Similarly, Cluster 4 genes were predicted to be regulated primarily by PU.1, Bcl-6, SP1, and c-Myc, again consistent with the enrichment of homeostatic and constitutive gene ontologies in this cluster. On the other hand, Stat1, NFkB, Bcl-6, IRF1, and PU.1 were predicted to regulate Cluster 3 genes that

were enriched in pro-inflammatory genes. These agree with previous publications that demonstrated critical roles for Stat1, NFκB, IRF1 (along with IRF8), and PU.1 in microglial activation (Rustenhoven et al., 2018; Smith et al., 2013).

To determine the enrichment patterns of homeostatic, pro-inflammatory DAM, and antiinflammatory DAM gene expression within each cluster, we mapped our previously published lists of homeostatic, pro-inflammatory DAM, anti-inflammatory DAM, and M1-like and M2-like gene lists (Srikant Rangaraju et al., 2018) to a 2D tSNE representation of the clusters (Figure 4a). We observed that clusters 2 and 4 were enriched with homeostatic and anti-inflammatory DAM genes, while cluster 3 was enriched with pro-inflammatory DAM genes and M1-like genes (Figure 4b). ERK was found to positively regulate several canonical DAM genes, including Ccl3, Ch25h, Spp1, Igf1, and Itgax (Supplementary Figure 3) and pro-inflammatory DAM genes, including Ccl2, Irf1, Tnf, Slamf9, and Cd69 (Supplementary Figure 4). We also calculated a synthetic eigenvalue to represent overall expression of homeostatic, anti-inflammatory DAM, and pro-inflammatory DAM profiles across each condition using previously identified hub genes (Kme>0.75) present in our NanoString dataset (Dai et al., 2018; Gao et al., 2019). We confirmed that inhibition of ERK suppresses homeostatic, anti-inflammatory, and pro-inflammatory DAM gene expression, while IFNy increases pro-inflammatory DAM and suppresses anti-inflammatory DAM gene expression (Figure 4c). A summary of the direction of regulation of each cluster by IFNy and ERK activity is shown in **Figure 4b** (Homeostatic [F(3,8)=29, n=3, p<0.001], Pro-inflammatory DAM [F(3,8)=29.5, n=3, p<0.001], Anti-inflammatory DAM [F(3,8)=22.4, n=3, p<0.001). We also performed qRT-PCR validation studies using primary mouse microglia to confirm ERK-mediated regulation of several DAM genes (Apoe [F(3,8)=25.79, n=3, p=0.002, SCH772984 vs. control post-hoc p=0.015], Trem2 [F(3,8)=4.79, n=3, p=0.034), Tyrobp [F(3,8)=8.45, n=3, p=0.007,

SCH772984 vs. Control post-hoc p=0.037], Spp1 [F(3,8)=80.52, n=3, p<0.001, SCH772984 vs. Control post-hoc p<0.001]) identified in Cluster 2 and a pro-inflammatory gene, Tnf (F(3,8)=5.20, n=3, p=0.028), identified in Cluster 3 (Supplementary Figure 5). Although ERK was found to positively regulate several clusters of microglial genes (Clusters 2, 3 and 4), we found that the magnitude of positive regulation by ERK was highest for Cluster 3 (Figure 4d) (F(3,8)=23.1, n=3, p<0.001, post-hoc p-value for Cluster 3 vs 2=0.030), which is enriched in pro-inflammatory DAM genes. Therefore, we hypothesized that ERK-dependent pathways disproportionately impact proinflammatory DAM gene expression over homeostatic and anti-inflammatory DAM gene expression. To test this hypothesis, we assessed effects of lower concentrations of the ERK inhibitor on expression of representative homeostatic, pro-inflammatory DAM, and antiinflammatory DAM genes. We found that ERK inhibition at dose ranges between 4-50 nM inhibited gene expression of Ptgs2, a pro-inflammatory DAM gene (IFNy-stimulated conditions: F(3,10)=9.09, n=3, p=0.002, IFNy+SCH772984 50nM vs. IFNy p<0.001) without impacting homeostatic (Tgfbr1, Bin1) or anti-inflammatory DAM genes (Spp1, Tyrobp) (Supplementary Figure 6).

To summarize our findings from transcriptomic and *in-vitro* microglial validation studies, ERK appears to be important for homeostatic, protective, and pathological responses mediated by microglia. However, the critical role for ERK in regulating pro-inflammatory immune responses appears to be most evident under pro-inflammatory conditions, suggesting that promotion of neuroinflammatory disease mechanisms via microglial ERK may be context dependent. While ERK activation in homeostatic microglia may regulate constitutive functions and mediate the effects of several trophic factors, ERK activation under disease-associated conditions, such as in AD, may regulate pro-inflammatory immune responses.

## ERK signaling regulates microglial phagocytic function.

Having found that ERK signaling regulates diverse DAM-associated genes, we next asked if ERK inhibition modulates microglial phagocytic function. To test this, we used a flow cytometric assay of fluorescently labeled AB42 fibril phagocytosis. We observed that ERK inhibition reduced microglial phagocytosis of Aβ42 fibrils regardless of stimulation by IFNγ (Figure 5a-b, F(3.8)=67.1, n=3 p<0.001, SCH772984 vs. control post-hoc p<0.001, IFNy+ SCH772984 vs. IFNy post-hoc p<0.001, control vs IFNy post-hoc p=0.959 Supplementary Figure 7). Since pro-inflammatory microglia can also mediate neurotoxicity via direct neuronal phagocytosis, we performed in-vitro microglia/neuronal co-culture studies and determined the effect of IFNy and ERK inhibition on microglia-mediated neuronal phagocytosis. N2a cells were stably transduced to express GFP and then differentiated with retinoic acid under low serum conditions for 4 days. Primary mouse microglia, which were treated with IFNy and/or the ERK inhibitor, were then added to differentiated N2a-GFP cells for another 24 h, after which microglia were collected for flow cytometry to measure GFP positivity within microglia (Figure 5c). First, we observed that addition of microglia, regardless of treatment, did not significantly decrease viability in N2a cells (**Figure 5d**, F(4,10)=1.36, n=3, p=0.314). Inhibition of ERK significantly reduced microglial phagocytosis of N2a cells without IFNy treatment (Figure 5e, F(3,8)=6.55, n=3, p=0.015, SCH772984 vs. control post-hoc p=0.017). These functional assays support a role for ERK in phagocytic activity, both for Aβ and neuronal phagocytosis.

GWAS and proteomic datasets reveal evidence for a pathophysiological role for ERK activation in human AD.

Upon finding ERK signaling can regulate microglial function, we searched for evidence of dysregulated ERK signaling human tissues. If ERK signaling in microglia is important in human AD pathogenesis, we predicted that ERK signaling should lie upstream of immune determinants of AD genetic risk. To test this hypothesis, we cross-referenced ERK regulated gene clusters generated from the NanoString analysis of mouse microglia against late-onset AD risk genes identified in meta-analyses of human GWAS studies, using an approach called Multi-marker Analysis of GenoMic Annotation (MAGMA) (de Leeuw, Mooij, Heskes, & Posthuma, 2015; Seyfried et al., 2017). MAGMA is a tool for gene and gene-set analysis of GWAS data that accounts for linkage disequilibrium and detects associations based on several markers, giving it distinct advantages over existing techniques (de Leeuw et al., 2015). Of over 1,000 known AD risk genes, 43 were present in the NanoString panel and 28 demonstrated differential expression in our dataset, mapping to any one of the 5 gene clusters (Figure 6a, Supplementary Table 7). While there was no statistically significant over-representation of AD risk genes in any of the clusters, risk genes with highest MAGMA significance mapped to Cluster 2 (Cnn2, Ms4a4a, Mef2c, Cd33) and Cluster 4 (Bin1, Pilra, Ep300). Cluster 3 AD risk genes included Sqstm1, Lrrc25 and Nrp2. Of these 28 ERK-regulated AD risk genes, 11 genes are specifically expressed in microglia (highlighted in Figure 6a with red asterisks).

Next, to determine whether MAPK pathway protein expression and phospho-signaling is altered in human AD, we investigated two post-mortem brain quantitative proteomic datasets. The clinical and demographic data for these study cohorts can be found in **Supplementary Table 1**. The first dataset was derived from 10 controls, 10 AD cases, 10 with Parkinson's disease, and 10 with both AD and Parkinson's disease pathological features (L. Ping et al., 2018). TMT proteomics was performed on tissues obtained from the dorsolateral pre-frontal cortex (**Supplementary Table** 

8)(Lingyan Ping et al., 2020). In this dataset, 33 MAPK proteins were identified and differential expression analyses comparing AD with control samples revealed increased expression of MAPK1 (ERK2) and MAPK3 (ERK1) in AD, while other MAPKs including MAPK8-10 (JNK1-3) were decreased in AD brains (Figure 6b). We also found that increased levels of MAPK3 (ERK1) (F(3,36)=6.61, n=10, p=0.001, post-hoc AD vs Control p=0.002, post-hoc AD-PD vs PD p=0.029) and MAPK1 (ERK2) (F(3,36)=5.04, n=10, p=0.005, post-hoc AD vs Control p=0.019, post-hoc AD-PD vs PD p=0.024) were only seen in brains with AD pathology, while Parkinson's disease brains did not exhibit increased MAPK1 or MAPK3 levels (Figure 6c-e). We also observed strong associations between AD neuropathological grade (Braak stage) and protein levels of MAPK1 (Spearman's R=0.56, p=0.003) and MAPK3 (Spearman's R=0.63, p<0.001) (Figure 6d, f). These findings show that ERK signaling proteins are specifically increased in AD brains. However, these total protein data do not confirm whether activation of ERK proteins are also increased.

We then turned to an existing phospho-proteomic dataset available on Synapse at <a href="https://www.synapse.org/#!Synapse:syn20820053/wiki/596078">https://www.synapse.org/#!Synapse:syn20820053/wiki/596078</a> in which frontal cortex samples from six controls, six asymptomatic AD pathology, and six symptomatic AD cases were used for quantitative TMT proteomics after purification of phosphopeptides on an immobilized metal affinity chromatography (IMAC) column (Lingyan Ping et al., 2020). Within this dataset, we obtained expression data for phosphopeptides that mapped to any of the known 60 MAPK family reference protein/gene list. This identified 127 phospho-peptides, of which 57 peptides showed differential expression (unadjusted ANOVA p<0.05) across the three conditions (Figure 7, Supplementary Table 9). K-means clustering of these differentially expressed peptides revealed distinct clusters with unique trajectories of change across stages of AD progression (control→AsymAD→AD) (Figure 7a). Cluster 1 consisted of peptides with dose-dependent

increase across the three groups, and Cluster 4 showed early and sustained increase, while Cluster 3 showed a delayed increase. Conversely, Clusters 2 showed decreased expression in clinical stages of AD pathology, although the number of these peptides was relatively small. The overall trajectories of change are presented in Figure 7b. Based on known biological functions of each MAPK protein, we found that 20 peptides (11 gene symbols) mapped to the ERK cascade, while 23 peptides (8 gene symbols) mapped to JNK, 8 peptides (3 gene symbols) mapped to p38, and 4 peptides mapped to MAPK proteins involved in cross talk between JNK and p38 MAPK cascades (Figure 7c). To gain further insights into roles of differentially expressed phosphopeptides in each signaling pathway, we then mapped each phosphopeptide to known MAPK signaling pathways. peptides ERK-related mapped all levels of the ERK signaling cascade to (RAF→MEK→MAPK→RSK) (Figure 7d). Within the 20 ERK-related phosphopeptides with differential expression in this dataset, we then identified key phosphosites in ERK-family proteins of AD relevance. Three RSK peptides (RPS6KA2 pS434 and pS402, and RPS6KA5 pS750) and RAF peptides (BRAF dual phosphorylated pS358+pS750 and ARAF pS157) were increased at least 1.5-fold in AD compared to controls, and 2 RSK phosphopeptides (RPS6KA2 pS434 and pS402) were also increased 1.5-fold in the asymptomatic stage of AD (Supplementary Table 9). Two phosphosites in ERK2 were also increased in AD (MAPK1/ERK2 pS284, MAPK1/ERK2 pS202). While little is known about pS284 and its impact on ERK activity, S202 in ERK2 is located at the activating lip in very close proximity to two phosphorylation sites that confer full ERK kinase activity (ERK2 T185/Y187), and a S202P mutation confers resistance to ERK inhibitors, suggesting that ERK phosphorylation at S202 may positively regulate ERK activation (Goetz, Ghandi, Treacy, Wagle, & Garraway, 2014). In addition to ERK phosphopeptides, we also found that early signaling events in the JNK and p38 cascades represented by phosphopeptides

were also differentially expressed in AD brains (**Supplementary Table 9**). To identify upstream triggers that may regulate these differentially expressed MAPK phosphopeptides in AD, we performed pathway enrichment analysis using PANTHER and found that the majority of proteins were downstream of growth factor receptors and RTKs such as PDGF, GnRH, FGF, EGF, TGF, and VEGF receptors (**Supplementary Table 10**) (Thomas et al., 2003). These findings using cross-sectional human post-mortem brain data show unique patterns of ERK activation in asymptomatic and symptomatic stages of AD pathology, suggesting that differential flux through MAPK signaling pathways, specifically ERK, may underlie symptomatic progression and neurodegeneration. We have summarized these patterns of differential ERK signaling observed in our phosphoproteomic analyses in **Figure 8**. Overall, ERK signaling activation in human AD brains was consistent with our observations in the 5xFAD mouse model of Aβ pathology of AD.

## **DISCUSSION**

Immune responses are orchestrated by early phospho-signaling events that follow activation of cell surface receptors. In turn, phospho-signaling results in regulated expression of groups of genes that together determine the immunological phenotype and function of the cell. Among the various immune signaling cascades that may regulate microglial functions, we focused on the MAPK family of signaling proteins in the 5xFAD pre-clinical AD model in order to identify pathologically relevant changes in MAPK signaling in microglia that may be responsible for pro-inflammatory immune activation in AD. Using Luminex analyses of phospho-proteins in acutely-isolated microglia, we found that among the three main classes of MAPKs, upregulated ERK signaling was the most apparent in microglia isolated from a mouse model of AD. However, no significant changes in MAPK activation were observed in whole tissue, suggesting that ERK

signaling may not be coordinated among different cell types in the brain and that ERK activation may be particularly characteristic of microglia in AD. Since ERK signaling is often transient following immune stimuli, our observation of significantly increased p-ERK1/2 levels in mouse microglia from an AD model also suggests that ERK activation may be persistently elevated in AD, potentially as a result of sustained activation of ERK via agonists of RTKs.

In support of a disease-relevant role for ERK in AD, we also found that ERK proteins are highly abundant in microglia isolated from 5xFAD mice. Moreover, in-vitro experiments using primary microglia revealed that inhibition of ERK strongly suppressed pro-inflammatory immune activation induced by IFNy, which is an AD relevant pro-inflammatory cytokine (Wood et al., 2015; Zheng, Zhou, & Wang, 2016). We also found that ERK signaling is important for homeostatic and anti-inflammatory gene expression, as well as constitutive microglial functions including phagocytosis of AB and neuronal phagocytosis, which is a potentially neurotoxic microglial function during AD pathogenesis (Rajendran & Paolicelli, 2018). ERK signaling was also found to be an upstream regulator of several canonical DAM genes, including Trem2 and Tyrobp, suggesting that ERK signaling may regulate the transition of homeostatic microglia to DAM, a phenotype commonly seen in AD and other neurodegenerative diseases. However, we did not observe any role for ERK signaling in regulation of microglial Apoe expression, suggesting that the Apoe-Trem2-dependent checkpoint for homeostatic-to-DAM transition in AD (Krasemann et al., 2017) may be regulated by both ERK-independent and ERK-dependent mechanisms. Interestingly, ERK activation was also upstream of several immune AD risk genes, including Cd33, Bin1, Plcg2, Trem2, and Cnn2, emphasizing the importance of ERK signaling in regulating immune pathways responsible for AD pathogenesis. While our in-vitro findings show that ERK is a positive regulator of homeostatic, pro-inflammatory and anti-inflammatory DAM

genes in microglia, the effect of ERK inhibition on pro-inflammatory DAM gene expression after induction by IFNy was far more profound than under unstimulated conditions, emphasizing a potential context-dependent effect of ERK-mediated gene regulation in microglia. Based on our in-vitro studies, the most robust effects of ERK inhibition seem to be suppression of IFNy-induced proinflammatory genes, many of which are detrimental in AD pathogenesis. However, there are several AD-associated genes with potentially protective and unclear roles which are also ERK dependent. These highlight a complex role for ERK in microglial activation. Another interpretation is that the level of ERK inhibition may determine the overall protective or detrimental phenotype of microglia. In support of this idea, we found that lower levels of ERK inhibition (closer to the known EC50s for ERK1 and 2) have a more robust effect on pro-inflammatory gene expression with no impact on homeostatic or inflammatory DAM gene expression. At high doses, all three gene profiles are affected, as seen in our Nanostring data although the effect of ERK inhibition was most marked in pro-inflammatory gene expression (cluster 3, Figures 3 and 4). While we have to explore this concept further, this raises the possibility that lower level ERK of inhibition (modulation) may be the desired approach *in-vivo*. One limitation of our work is that all *in-vitro* experiments were conducted using microglia derived from neonatal mouse pups due to challenges of keeping adult microglia alive in culture, limiting our ability to generalize the observed effects of ERK signaling to microglia from adult or aging mice.

Consistent with these important roles for ERK signaling in mouse microglia and in 5xFAD mice, we found that human AD is also characterized by increased ERK activation. Our analyses of human proteomics data, including phospho-proteomics studies, confirmed that ERK1 and 2 are the only two MAPKs that are increased at the total protein level in human AD brains, while other MAPKs, such as JNKs, are decreased. At the phospho-protein level, 57 MAPK phosphopeptides

were found to be differentially expressed in human AD brains, and the relative proportion of ERK proteins with differentially expressed phosphopeptides was highest compared to other MAPK proteins. A limitation of this analysis is that human post-mortem proteomic data was not cell type specific, while our mouse Luminex findings confirmed microglia-specific ERK activation in 5xFAD mice. This limits our ability to determine whether ERK and other MAPK-related changes occurring in 5xFAD microglia also occur in human microglia in AD cases, and whether MAPK changes observed in the human brain proteomes are driven by microglia or by other cell types. Future human brain cell type-specific analysis may address these questions. Overall, our integrated analyses of signaling data obtained from pre-clinical 5xFAD mice and *in-vitro* mechanistic studies in microglia along with confirmatory human post-mortem brain proteomics findings strongly support an important role for ERK signaling in AD pathogenesis.

From a therapeutic perspective, our results suggest that inhibition of ERK in microglia should limit pro-inflammatory disease mechanisms. They also highlight, however, the importance of ERK in homeostasis and constitutive cellular functions, such as cell division, survival, and phagocytosis. Furthermore, ERK is ubiquitously expressed in the brain in several cell types and is also important in neuronal physiological functions, including learning and memory (Hutton et al., 2017; Silingardi et al., 2011). Therefore, therapeutic inhibition of ERK signaling specifically in microglia will likely be limited by cellular non-selectivity, potentially resulting in undesired side effects. Rather than global inhibition of ERK activation, another potential strategy to attain desirable neuro-immunomodulatory effects would be to modulate microglial RTKs that primarily signal via ERK. In recent work, several RTKs were indeed identified as unique to homeostatic (CSF1R, MERTK), pro-inflammatory DAM (FLT4), and anti-inflammatory DAM (AXL, FLT3, IGF1R), among others (Fourgeaud et al., 2016; Srikant Rangaraju et al., 2018). If different RTKs

activate ERK in distinct manners, each resulting in expression of distinct gene sets, the dynamics of ERK signaling downstream of RTKs are likely to modulate downstream gene expression, although this has yet to be explored in microglia. Strategically manipulating ERK signaling via RTKs could allow for the targeted suppression of pro-inflammatory DAM genes with known detrimental roles in AD, while sparing or even augmenting protective homeostatic and anti-inflammatory DAM genes, resulting in a net beneficial immune response. Based on our results, future studies will investigate RTK-specific MAPK signaling in microglia in AD models to guide therapeutic interventions.

A dynamic model of ERK activation in microglia also raises the intriguing possibility that short-term ERK activation regulates homeostatic and constitutive responses, while sustained and long-term ERK activation may mediate disease-associated and pro-inflammatory microglial responses in neurodegeneration. Indeed, *in-vitro* and *in-vivo* studies using real-time ERK signaling reporters in neuronal cells and T cells have shown that the immune effects of short-term ERK activation and sustained ERK activation are very different (de la Cova, Townley, Regot, & Greenwald, 2017; Harvey et al., 2008; Konishi et al., 2018). The recent development of FRET-based biosensors of ERK and MAPK signaling will allow us to test mechanistic hypotheses to define the ERK signaling dynamics of diverse RTKs expressed by microglia, and then further determine the downstream effects of ERK activation via RTKs on gene expression patterns both *in-vitro* and *in-vivo*. These novel approaches will also facilitate the development of novel approaches to regulate ERK signaling dynamics to achieve desired neuroinflammatory microglial phenotypes.

Although we focused on ERK signaling, our Luminex studies were consistent with prior work revealing increased activation of p38 and trends towards increased JNK activation in

microglia from 5xFAD mice, and human post-mortem brain proteomes also suggested activation of JNK and p38 pathways, although to a lesser extent than ERK (Lee & Kim, 2017; Yarza et al., 2016). These data suggest that non-ERK MAPKs may also be relevant in regulating microglial functions in AD. Beyond these MAPKs, NFkB signaling is another key regulator of proinflammatory immune responses, which was not considered in our studies (Shih, Wang, & Yang, 2015). Unlike the robust effects of ERK inhibition observed in these studies, we previously found that inhibition of JNK or NFkB in microglia had minimal effects on the expression of selected homeostatic and DAM genes or on effects of pro-inflammatory stimuli in microglia (Gao et al., 2019). Due to the limited yield of protein from acutely-isolated CD11b<sup>+</sup> microglia from adult mice, we focused our efforts on ERK, although future studies will investigate the importance of other MAPKs, specifically p38 and JNK signaling pathways, in AD. Another limitation of our work include low protein yields that limited our ability to explore regional differences in microglial ERK activation in 5xFAD mice. Lastly, a serious limitation of our study includes the fact that some invitro experiments were conducted with only three biological replicates per group. As a result, findings from these must be interpreted with great caution. At the time these experiments were completed and during the peer review period, additional replicates were not available and additional experiments could not be performed due to limited laboratory staffing and access due to the ongoing COVID19 pandemic.

### **CONCLUSIONS**

In conclusion, our integrated analysis of a pre-clinical model of AD pathology, *in-vitro* transcriptomic and functional studies in primary microglia, and human proteomic data provide

novel insights into ERK activation in AD pathogenesis. Moreover, they suggest that modulation of ERK phosphorylation may be a novel avenue for immunomodulation in AD.

### **CONFLICT OF INTEREST**

The authors report no competing interests

## **FUNDING**

This study was supported by the Alzheimer's Association AARG 37102 (PI: Rangaraju), NIH K08-NS099474-1 and 1R01NS114130-01A1 (PI: Rangaraju), the Accelerating Medicine Partnership for Alzheimer's Disease (U01 AG046161 and U01 AG061357, PI: Levey), the Emory Alzheimer's Disease Research Center (P50 AG025688, Pilot award to S.R. and L.B.W) and P30 AG066511(PI: Levey), and by startup funds from the George W. Woodruff School of Mechanical Engineering at the Georgia Institute of Technology (Wood). L.B.W. was supported in part by the National Institutes of Health Cell and Tissue Engineering Biotechnology Training Grant (T32-GM008433) and National Science Foundation CAREER Award 1944053. This study was supported in part by the Emory Flow Cytometry Core (EFCC), one of the Emory Integrated Core Facilities (EICF) and is subsidized by the Emory University School of Medicine. Additional support was provided by the Georgia Clinical & Translational Science Alliance of the NIH under Award Number UL1TR002378. The content is solely the responsibility of the authors and does not necessarily reflect the official views of the NIH.

## **AUTHOR CONTRIBUTIONS**

MJC, SRamesha, LW and SRangaraju designed the study, and analyzed and interpreted the results. MJC, SRamesha, LDW, LW, TG, HX, LP, EBD and DD conducted the experiments. AIL, NTS, JJL and LP provided the human brain proteomic data for analysis. MJC, SRangaraju and LW wrote the article. All authors contributed to the article. SRangaraju and LW supervised the project.

**Data Accessibility:** Raw data from both proteomic datasets are publicly available (Dataset 1: <a href="http://proteomecentral.proteomexchange.org/cgi/GetDataset?ID=PXD007160">http://proteomecentral.proteomexchange.org/cgi/GetDataset?ID=PXD007160</a>; Dataset 2: deposited at <a href="https://www.synapse.org/#!Synapse:syn20820053/wiki/596078">https://www.synapse.org/#!Synapse:syn20820053/wiki/596078</a>). Supplementary data files pertinent to this manuscript are also provided within the manuscript.

## SUPPLEMENTARY INFORMATION

This manuscript contains 7 Supplementary Figures

Supplementary Figure 1. MAPK phospho-signaling changes in frontal cortex in WT and 5xFAD mouse brain.

Supplementary Figure 2. ERK inhibition exerts minimal impact on viability of microglia.

Supplementary Figure 3. DAM genes positively regulated by ERK signaling.

Supplementary Figure 4. Pro-inflammatory DAM genes positively regulated by ERK signaling

Supplementary Figure 5. qRT-PCR validation confirms ERK effect of select DAM genes.

Supplementary Figure 6. qRT-PCR study showing dose-dependent regulation of pro-

inflammatory DAM but not homeostatic and anti-inflammatory DAM genes by ERK inhibition in primary microglia.

Supplementary Figure 7. Flow cytometry gating strategy for live/dead cell distinction.

This manuscript contains 10 Supplementary Tables

Supplementary Table 1. Clinical data for human post-mortem brain samples

Supplementary Table 2. List of MAPK genes/proteins cross-referenced with published proteomic data sets.

Supplementary Table 3. NanoString transcriptomic dataset for 678 genes with ANOVA p values.

Supplementary Table 4. K-means clustering of 465 differentially expressed genes in NanoString dataset.

Supplementary Table 5. Gene Ontology analysis of K-means clusters showing enriched GO terms, KEGG, and Wikipathways.

Supplementary Table 6. Transcription factors downstream of ERK activation likely to regulate genes in clusters 2,3, and 4.

Supplementary Table 7. MAGMA analysis of 28 known Alzheimer's disease risk genes differentially expressed in NanoString dataset.

Supplementary Table 8. Human frontal cortex proteomics from Alzheimer's disease, Alzheimer's disease, Parkinson's disease, Parkinson's disease, and control brains.

Supplementary Table 9. Differentially expressed ERK, JNK, and p38 phosphopeptides from human frontal cortex samples.

Supplementary Table 10. Upstream regulators of differentially expressed MAPK phosphopeptides in Alzheimer's disease.

## REFERENCES

- Arkun, Y., & Yasemi, M. (2018). Dynamics and control of the ERK signaling pathway: Sensitivity, bistability, and oscillations. *PLoS One,* 13(4), e0195513. doi:10.1371/journal.pone.0195513
- Bachiller, S., Jimenez-Ferrer, I., Paulus, A., Yang, Y., Swanberg, M., Deierborg, T., & Boza-Serrano, A. (2018). Microglia in Neurological Diseases: A Road Map to Brain-Disease Dependent-Inflammatory Response. *Front Cell Neurosci*, *12*, 488. doi:10.3389/fncel.2018.00488
- Block, M. L., Zecca, L., & Hong, J. S. (2007). Microglia-mediated neurotoxicity: uncovering the molecular mechanisms. *Nat Rev Neurosci*, 8(1), 57-69. doi:10.1038/nrn2038
- Cargnello, M., & Roux, P. P. (2011). Activation and function of the MAPKs and their substrates, the MAPK-activated protein kinases. *Microbiol Mol Biol Rev*, 75(1), 50-83. doi:10.1128/MMBR.00031-10
- Dai, J., Johnson, E. C. B., Dammer, E. B., Duong, D. M., Gearing, M., Lah, J. J., . . . Seyfried, N. T. (2018). Effects of APOE Genotype on Brain Proteomic Network and Cell Type Changes in Alzheimer's Disease. *Frontiers in Molecular Neuroscience,* 11(454). doi:10.3389/fnmol.2018.00454
- Dammer, E. B., Lee, A. K., Duong, D. M., Gearing, M., Lah, J. J., Levey, A. I., & Seyfried, N. T. (2015). Quantitative phosphoproteomics of Alzheimer's disease reveals cross-talk between kinases and small heat shock proteins. *Proteomics*, 15(2-3), 508-519. doi:10.1002/pmic.201400189
- de la Cova, C., Townley, R., Regot, S., & Greenwald, I. (2017). A Real-Time Biosensor for ERK Activity Reveals Signaling Dynamics during C. elegans Cell Fate Specification. Developmental cell, 42(5), 542-553.e544. doi:10.1016/j.devcel.2017.07.014
- de Leeuw, C. A., Mooij, J. M., Heskes, T., & Posthuma, D. (2015). MAGMA: Generalized Gene-Set Analysis of GWAS Data. *PLOS Computational Biology, 11*(4), e1004219. doi:10.1371/journal.pcbi.1004219
- Dubbelaar, M. L., Kracht, L., Eggen, B. J. L., & Boddeke, E. (2018). The Kaleidoscope of Microglial Phenotypes. *Front Immunol*, *9*, 1753. doi:10.3389/fimmu.2018.01753
- Fourgeaud, L., Través, P. G., Tufail, Y., Leal-Bailey, H., Lew, E. D., Burrola, P. G., . . . Lemke, G. (2016). TAM receptors regulate multiple features of microglial physiology. *Nature*, 532(7598), 240-244. doi:10.1038/nature17630
- Gao, T., Jernigan, J., Raza, S. A., Dammer, E. B., Xiao, H., Seyfried, N. T., . . . Rangaraju, S. (2019). Transcriptional regulation of homeostatic and disease-associated-microglial genes by IRF1, LXRβ, and CEBPα. *Glia*, *67*(10), 1958-1975. doi:10.1002/glia.23678
- Geraghty, A. C., Gibson, E. M., Ghanem, R. A., Greene, J. J., Ocampo, A., Goldstein, A. K., . . . Monje, M. (2019). Loss of Adaptive Myelination Contributes to Methotrexate Chemotherapy-Related Cognitive Impairment. *Neuron*, *103*(2), 250-265 e258. doi:10.1016/j.neuron.2019.04.032
- Goetz, E. M., Ghandi, M., Treacy, D. J., Wagle, N., & Garraway, L. A. (2014). ERK Mutations Confer Resistance to Mitogen-Activated Protein Kinase Pathway Inhibitors. *Cancer Research*, 74(23), 7079-7089. doi:10.1158/0008-5472.Can-14-2073
- Hagemeyer, N., Hanft, K. M., Akriditou, M. A., Unger, N., Park, E. S., Stanley, E. R., . . . Prinz, M. (2017). Microglia contribute to normal myelinogenesis and to oligodendrocyte progenitor

- maintenance during adulthood. *Acta Neuropathol, 134*(3), 441-458. doi:10.1007/s00401-017-1747-1
- Harvey, C. D., Ehrhardt, A. G., Cellurale, C., Zhong, H., Yasuda, R., Davis, R. J., & Svoboda, K. (2008).

  A genetically encoded fluorescent sensor of ERK activity. *Proceedings of the National Academy of Sciences*, 105(49), 19264-19269. doi:10.1073/pnas.0804598105
- Hickman, S., Izzy, S., Sen, P., Morsett, L., & El Khoury, J. (2018). Microglia in neurodegeneration. *Nat Neurosci*, *21*(10), 1359-1369. doi:10.1038/s41593-018-0242-x
- Hutton, S. R., Otis, J. M., Kim, E. M., Lamsal, Y., Stuber, G. D., & Snider, W. D. (2017). ERK/MAPK Signaling Is Required for Pathway-Specific Striatal Motor Functions. *The Journal of Neuroscience*, *37*(34), 8102-8115. doi:10.1523/jneurosci.0473-17.2017
- Keren-Shaul, H., Spinrad, A., Weiner, A., Matcovitch-Natan, O., Dvir-Szternfeld, R., Ulland, T. K., . . . Amit, I. (2017). A Unique Microglia Type Associated with Restricting Development of Alzheimer's Disease. *Cell*, 169(7), 1276-1290.e1217. doi:10.1016/j.cell.2017.05.018
- Kim, S. H., Smith, C. J., & Van Eldik, L. J. (2004). Importance of MAPK pathways for microglial proinflammatory cytokine IL-1 beta production. *Neurobiol Aging*, *25*(4), 431-439. doi:10.1016/S0197-4580(03)00126-X
- Konishi, Y., Terai, K., Furuta, Y., Kiyonari, H., Abe, T., Ueda, Y., . . . Matsuda, M. (2018). Live-Cell FRET Imaging Reveals a Role of Extracellular Signal-Regulated Kinase Activity Dynamics in Thymocyte Motility. *iScience*, 10, 98-113. doi: <a href="https://doi.org/10.1016/j.isci.2018.11.025">https://doi.org/10.1016/j.isci.2018.11.025</a>
- Krasemann, S., Madore, C., Cialic, R., Baufeld, C., Calcagno, N., El Fatimy, R., . . . Butovsky, O. (2017). The TREM2-APOE Pathway Drives the Transcriptional Phenotype of Dysfunctional Microglia in Neurodegenerative Diseases. *Immunity*, 47(3), 566-581.e569. doi:10.1016/j.immuni.2017.08.008
- Lambert, J. C., Ibrahim-Verbaas, C. A., Harold, D., Naj, A. C., Sims, R., Bellenguez, C., . . . Amouyel, P. (2013). Meta-analysis of 74,046 individuals identifies 11 new susceptibility loci for Alzheimer's disease. *Nat Genet*, 45(12), 1452-1458. doi:10.1038/ng.2802
- Lee, J. K., & Kim, N.-J. (2017). Recent Advances in the Inhibition of p38 MAPK as a Potential Strategy for the Treatment of Alzheimer's Disease. *Molecules (Basel, Switzerland), 22*(8), 1287. doi:10.3390/molecules22081287
- Liddelow, S. A., Guttenplan, K. A., Clarke, L. E., Bennett, F. C., Bohlen, C. J., Schirmer, L., . . . Barres, B. A. (2017). Neurotoxic reactive astrocytes are induced by activated microglia. *Nature*, 541(7638), 481-487. doi:10.1038/nature21029
- Mastrangelo, M. A., Sudol, K. L., Narrow, W. C., & Bowers, W. J. (2009). Interferon-{gamma} differentially affects Alzheimer's disease pathologies and induces neurogenesis in triple transgenic-AD mice. *Am J Pathol*, *175*(5), 2076-2088. doi:10.2353/ajpath.2009.090059
- Morris, E. J., Jha, S., Restaino, C. R., Dayananth, P., Zhu, H., Cooper, A., . . . Samatar, A. A. (2013). Discovery of a Novel ERK Inhibitor with Activity in Models of Acquired Resistance to BRAF and MEK Inhibitors. *Cancer Discovery*, *3*(7), 742-750. doi:10.1158/2159-8290.Cd-13-0070
- Namsi, A., Nury, T., Hamdouni, H., Yammine, A., Vejux, A., Vervandier-Fasseur, D., . . . Lizard, G. (2018). Induction of Neuronal Differentiation of Murine N2a Cells by Two Polyphenols Present in the Mediterranean Diet Mimicking Neurotrophins Activities: Resveratrol and Apigenin. *Diseases*, 6(3), 67.

- Ping, L., Duong, D. M., Yin, L., Gearing, M., Lah, J. J., Levey, A. I., & Seyfried, N. T. (2018). Global quantitative analysis of the human brain proteome in Alzheimer's and Parkinson's Disease. *Sci Data*, *5*, 180036. doi:10.1038/sdata.2018.36
- Ping, L., Kundinger, S. R., Duong, D. M., Yin, L., Gearing, M., Lah, J. J., . . . Seyfried, N. T. (2020). Global quantitative analysis of the human brain proteome and phosphoproteome in Alzheimer's disease. *Scientific Data*, 7(1), 315. doi:10.1038/s41597-020-00650-8
- R Core Team. (2020). R: A Language and Environment for Statistical Computing. Vienna, Austria: R Foundation for Statistical Computing. Retrieved from <a href="https://www.r-project.org/">https://www.r-project.org/</a>
- Rajendran, L., & Paolicelli, R. C. (2018). Microglia-Mediated Synapse Loss in Alzheimer's Disease. *The Journal of Neuroscience, 38*(12), 2911-2919. doi:10.1523/jneurosci.1136-17.2017
- Rangaraju, S., Dammer, E. B., Raza, S. A., Gao, T., Xiao, H., Betarbet, R., . . . Seyfried, N. T. (2018). Quantitative proteomics of acutely-isolated mouse microglia identifies novel immune Alzheimer's disease-related proteins. *Mol Neurodegener*, *13*(1), 34. doi:10.1186/s13024-018-0266-4
- Rangaraju, S., Dammer, E. B., Raza, S. A., Rathakrishnan, P., Xiao, H., Gao, T., . . . Levey, A. I. (2018). Identification and therapeutic modulation of a pro-inflammatory subset of disease-associated-microglia in Alzheimer's disease. *Molecular Neurodegeneration*, 13(1), 24. doi:10.1186/s13024-018-0254-8
- Rangaraju, S., Raza, S. A., Li, N. X., Betarbet, R., Dammer, E. B., Duong, D., . . . Levey, A. I. (2018). Differential Phagocytic Properties of CD45(low) Microglia and CD45(high) Brain Mononuclear Phagocytes-Activation and Age-Related Effects. *Front Immunol, 9,* 405. doi:10.3389/fimmu.2018.00405
- Rustenhoven, J., Smith, A. M., Smyth, L. C., Jansson, D., Scotter, E. L., Swanson, M. E. V., . . . Dragunow, M. (2018). PU.1 regulates Alzheimer's disease-associated genes in primary human microglia. *Molecular Neurodegeneration*, *13*(1), 44-44. doi:10.1186/s13024-018-0277-1
- Santos, S. D., Verveer, P. J., & Bastiaens, P. I. (2007). Growth factor-induced MAPK network topology shapes Erk response determining PC-12 cell fate. *Nat Cell Biol, 9*(3), 324-330. doi:10.1038/ncb1543
- Sellgren, C. M., Gracias, J., Watmuff, B., Biag, J. D., Thanos, J. M., Whittredge, P. B., . . . Perlis, R. H. (2019). Increased synapse elimination by microglia in schizophrenia patient-derived models of synaptic pruning. *Nat Neurosci, 22*(3), 374-385. doi:10.1038/s41593-018-0334-7
- Seyfried, N. T., Dammer, E. B., Swarup, V., Nandakumar, D., Duong, D. M., Yin, L., . . . Levey, A. I. (2017). A Multi-network Approach Identifies Protein-Specific Co-expression in Asymptomatic and Symptomatic Alzheimer's Disease. *Cell systems, 4*(1), 60-72.e64. doi:10.1016/j.cels.2016.11.006
- Shih, R.-H., Wang, C.-Y., & Yang, C.-M. (2015). NF-kappaB Signaling Pathways in Neurological Inflammation: A Mini Review. *Frontiers in Molecular Neuroscience*, 8, 77-77. doi:10.3389/fnmol.2015.00077
- Silingardi, D., Angelucci, A., De Pasquale, R., Borsotti, M., Squitieri, G., Brambilla, R., . . . Berardi, N. (2011). ERK Pathway Activation Bidirectionally Affects Visual Recognition Memory and Synaptic Plasticity in the Perirhinal Cortex. *Frontiers in Behavioral Neuroscience*, *5*(84). doi:10.3389/fnbeh.2011.00084

- Smith, A. M., Gibbons, H. M., Oldfield, R. L., Bergin, P. M., Mee, E. W., Faull, R. L. M., & Dragunow, M. (2013). The transcription factor PU.1 is critical for viability and function of human brain microglia. *Glia*, *61*(6), 929-942. doi:10.1002/glia.22486
- Tay, T. L., Mai, D., Dautzenberg, J., Fernandez-Klett, F., Lin, G., Sagar, . . . Prinz, M. (2017). A new fate mapping system reveals context-dependent random or clonal expansion of microglia. *Nat Neurosci, 20*(6), 793-803. doi:10.1038/nn.4547
- Thomas, P. D., Campbell, M. J., Kejariwal, A., Mi, H., Karlak, B., Daverman, R., . . . Narechania, A. (2003). PANTHER: a library of protein families and subfamilies indexed by function. *Genome research*, 13(9), 2129-2141. doi:10.1101/gr.772403
- Wood, L. B., Winslow, A. R., Proctor, E. A., McGuone, D., Mordes, D. A., Frosch, M. P., . . . Haigis, K. M. (2015). Identification of neurotoxic cytokines by profiling Alzheimer's disease tissues and neuron culture viability screening. *Scientific reports*, 5, 16622-16622. doi:10.1038/srep16622
- Yarza, R., Vela, S., Solas, M., & Ramirez, M. J. (2016). c-Jun N-terminal Kinase (JNK) Signaling as a Therapeutic Target for Alzheimer's Disease. *Frontiers in pharmacology, 6,* 321-321. doi:10.3389/fphar.2015.00321
- Yates, B., Braschi, B., Gray, K. A., Seal, R. L., Tweedie, S., & Bruford, E. A. (2017). Genenames.org: the HGNC and VGNC resources in 2017. *Nucleic Acids Res, 45*(D1), D619-D625. doi:10.1093/nar/gkw1033
- Zambon, A. C., Gaj, S., Ho, I., Hanspers, K., Vranizan, K., Evelo, C. T., . . . Salomonis, N. (2012). GO-Elite: a flexible solution for pathway and ontology over-representation. *Bioinformatics* (Oxford, England), 28(16), 2209-2210. doi:10.1093/bioinformatics/bts366
- Zhang, W., & Liu, H. T. (2002). MAPK signal pathways in the regulation of cell proliferation in mammalian cells. *Cell Res*, *12*(1), 9-18. doi:10.1038/sj.cr.7290105
- Zheng, C., Zhou, X.-W., & Wang, J.-Z. (2016). The dual roles of cytokines in Alzheimer's disease: update on interleukins, TNF- $\alpha$ , TGF- $\beta$  and IFN- $\gamma$ . *Translational Neurodegeneration*, 5(1), 7. doi:10.1186/s40035-016-0054-4
- Zhou, X., Zoller, T., Krieglstein, K., & Spittau, B. (2015). TGFbeta1 inhibits IFNgamma-mediated microglia activation and protects mDA neurons from IFNgamma-driven neurotoxicity. *J Neurochem*, 134(1), 125-134. doi:10.1111/jnc.13111

Table 1. Antibody list and details

Name	Host	Vendor and RRID	<b>Immunizing Agent</b>	Dilution	Class
CD45	Rat	BD Biosciences,	Mouse thymus and	1:100	Monoclonal
(Flow		#552848	spleen		
cytometry)		RRID:AB_394489			
CD11b	Rat	BD Biosciences,	Mouse spleen	1:100	Monoclonal
(Flow		#557657			
cytometry)		RRID:AB_396772			
Phospho-	Rabbit	Cell Signaling	Residues on human	1:100	Polyclonal
ERK1/2		Technology, #9101S	ERK1/2		
(Flow		RRID:AB_331646	surrounding		
cytometry)			Thr202/Tyr204		
ERK1/2	Rabbit	R&D Systems,	E. coli-derived	1:20	Polyclonal
(Flow		AF1576	recombinant human		
cytometry)		RRID:AB_354872	ERK1/2		

#### FIGURE LEGENDS

# Figure 1. Increased activation of ERK1/2 and p38 MAPK signaling in microglia in the 5xFAD mouse Alzheimer's disease model.

- (a) Schematic summarizing key MAPK signaling pathways including ERK1/2, p38, and JNK signaling cascades, the three families of MAPKs, all of which result in the activation of transcription factors which regulate gene regulation.
- (b) Experimental outline for Luminex studies of acutely-isolated CD11b<sup>+</sup> CNS myeloid cells and frontal cortex brain samples isolated from age-matched WT and 5xFAD mice (n=7-8 mice/group). CD11b<sup>+</sup> cells were isolated by Percoll density centrifugation followed by CD11b enrichment using MACS columns. \*p<0.05, \*\*p<0.01, \*\*\*p<0.005.

(c) Summary of phospho-protein signaling data for phospho-ERK1/2 (p-ERK1/2), p-p38, and p-JNK signaling cascades in CD11b<sup>+</sup> CNS myeloid cells from WT and 5xFAD mice. Mean and SD of the expression of phospho (p)-proteins, as represented by the intensity of fluorescence, are represented. \*p<0.05, \*\*p<0.01, \*\*\*p<0.005

### Figure 2. Confirmation of increased ERK1/2 activation in 5xFAD microglia.

- (a-b) Bar plot showing the relative abundance of 17 MAPK proteins as compared to non-MAPK proteins in microglia from WT, 5xFAD, and LPS-treated WT mice (a) and BV2 microglia (b) using published proteomic datasets.
- (c) Differentially expressed MAPK proteins identified in PBS-treated WT, 5xFAD, and LPS-treated WT mice. Error bars represent SD. Proteins differentially expressed across groups (ANOVA p<0.05) and meeting statistical significance (post-hoc Tukey's HSD p<0.05) as compared to the WT-PBS group, are indicated. \*p<0.05, \*\*p<0.01, \*\*\*p<0.005.
- (d) Intra-cellular flow cytometric analysis of acutely-isolated CNS myeloid cells for p-ERK1/2 labeling. Gating strategy used is shown (top).
- (e) Quantitative analyses of flow cytometric studies of p-ERK1/2 and total ERK1/2 expression in WT and 5xFAD CD11b<sup>+</sup> CD45int microglia. \*p<0.05, \*\*p<0.01, \*\*\*p<0.005.

# Figure 3. Transcriptomic profiling of microglia reveals distinct clusters of genes regulated by ERK1/2.

(a) Heatmap showing K-means clustering analysis of 465 genes with differential expression across 4 treatment groups, as identified by one-way ANOVA, using Nanostring gene expression data.

Cluster 1: inhibited by ERK; Cluster 2: activated by ERK and inhibited by IFNy; Cluster 3: activated by ERK and IFNy; Cluster 4: inhibited by ERK.

(b) Gene Ontology (GO) analysis depicting enrichment of GO terms in genes belonging to each cluster.

## Figure 4. ERK1/2 positively regulates homeostatic, anti-inflammatory DAM, and proinflammatory DAM gene expression in microglia.

- (a) t-SNE plots showing clusters of genes based on Nanostring expression data. Color coders indicate K-means clusters identified in Figure 3. Clusters 2, 3 and 4 are positively regulated by ERK while cluster 1 is negatively regulated by ERK.
- (b) Distribution of homeostatic, pro-inflammatory DAM, anti-inflammatory DAM, M1-like, and M2-like microglial genes in each cluster.
- (c) Expression of synthetic eigengenes of each microglial state (homeostatic, pro-inflammatory DAM and anti-inflammatory DAM) across experimental conditions.
- (d) Plot showing the magnitude of change in overall gene expression level in each cluster (averaging across normalized gene expression within each cluster) between ERK inhibitor treated and non-treated conditions, in IFNγ stimulated conditions. N=3 replicates per group (Error bars represent SD). \*p<0.05, \*\*p<0.01, \*\*\*p<0.005 based on Tukey HSD post-hoc pairwise comparisons.

Figure 5. Roles of ERK activity in regulating microglial phagocytosis of fibrillar  $A\beta42$  and of neuronal phagocytosis.

- (a) Flow cytometry experimental data showing the uptake of fluorescent Aβ42 fibrils by live CD45<sup>+</sup> microglia that had been treated with an ERK1/2 inhibitor and/or IFNγ.
- (b) Bar graphs showing the reduction of microglial phagocytosis of Aβ42 by ERK inhibition under unstimulated and stimulated conditions in-vitro. N=3 replicates per group. Error bars represent SD. \*p<0.05, \*\*p<0.01, \*\*\*p<0.005.
- (c) Experimental protocol for microglia-N2a co-culture study: GFP-positive N2a cells were differentiated for 4 days using retinoic acid. Meanwhile, primary microglia were isolated, and after 24 hours, were incubated with the ERK inhibitor with or without IFNγ. After incubation for 24 hours, the microglia were seeded into the differentiated N2a cultures overnight and then harvested for antibody staining and flow cytometry. This figure was created using modified images from Servier Medical Art.
- (d) Bar plot demonstrating the viability of N2a cells when co-cultured with microglia. N=3 replicates per group. Error bars represent SD. \*p<0.05, \*\*p<0.01, \*\*\*p<0.005.
- (e) Bar graphs showing a reduction of microglial phagocytosis of differentiated N2a cells in the ERK inhibited group. GFP<sup>+</sup> N2A cells were differentiated and then co-cultured with primary microglia that were pre-treated with an ERK inhibitor with or without IFNγ. N=3 replicates per group. Error bars represent SD. \*p<0.05, \*\*p<0.01, \*\*\*p<0.005.

### Figure 6. MAGMA and TMT proteomics reveals role for ERK activation in human AD.

- (a) tSNE plot showing late-onset Alzheimer's disease risk genes identified in human GWAS analyses that are present in mouse microglia from the NanoString dataset (\*p < 0.05).
- (b) Differential expression analysis of human frontal cortex proteomes showing that MAPK1 (ERK2) and MAPK3 (ERK1), both shown in red, are expressed more highly in Alzheimer's

disease brains than in control brains while the opposite trend is observed in other notable MAPKs, shown in blue.

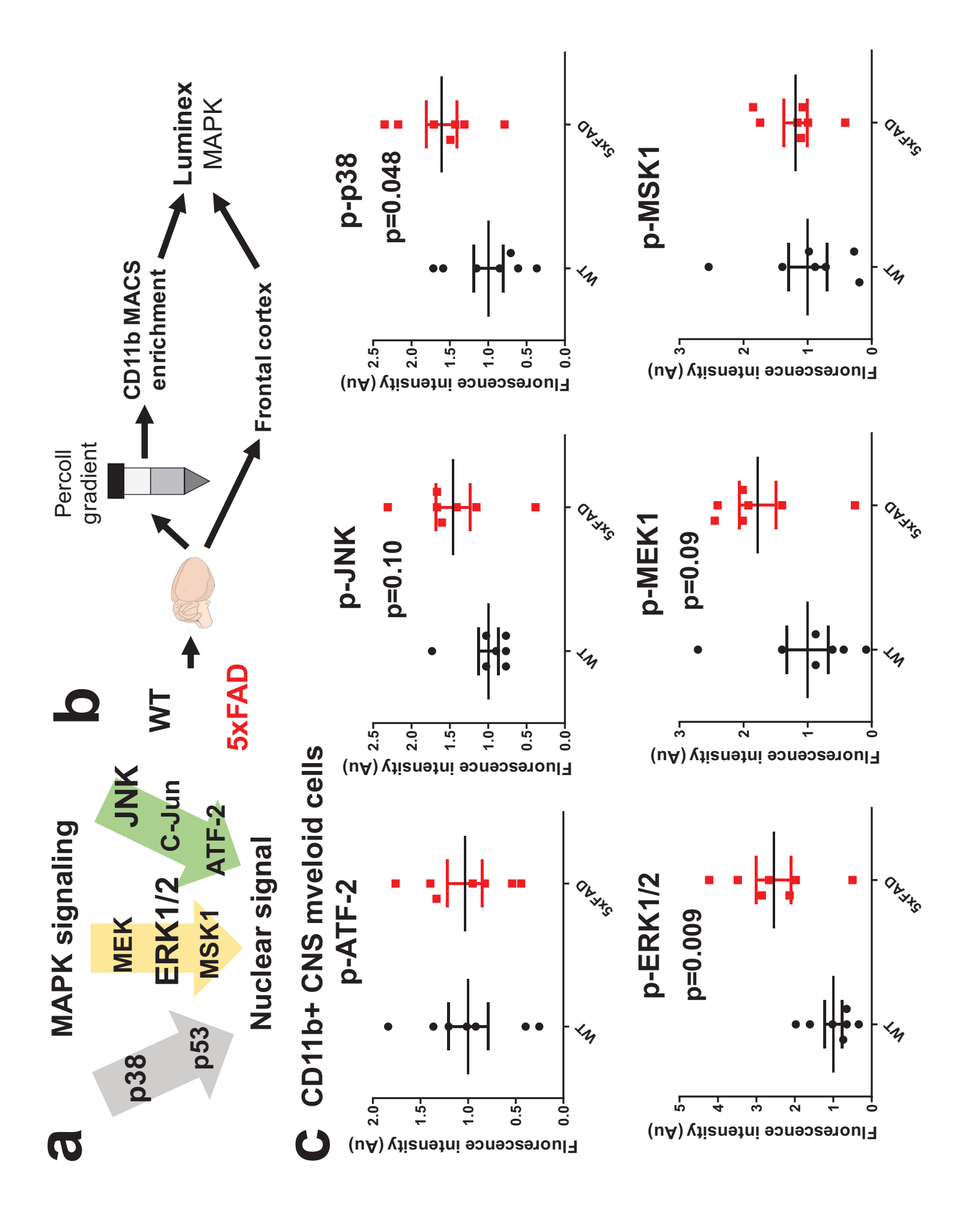
- (c) Box plots (median, min to max range and individual values) showing that MAPK3 expression levels are increased in Alzheimer's disease and Alzheimer's disease/Parkinson's disease brains as compared to Parkinson's disease or control brains (n=10 per group).
- (d) Correlation between Alzheimer's disease Braak stage and MAPK3 expression. Spearman's R and p-value are indicated.
- (e) Box plots (median, min to max range and individual values) showing that MAPK1 expression levels are increased in brains with Alzheimer's disease pathology (n=10 per group).
- (f) Correlation between Braak stage and MAPK1 expression. Spearman's R and p-value are indicated.

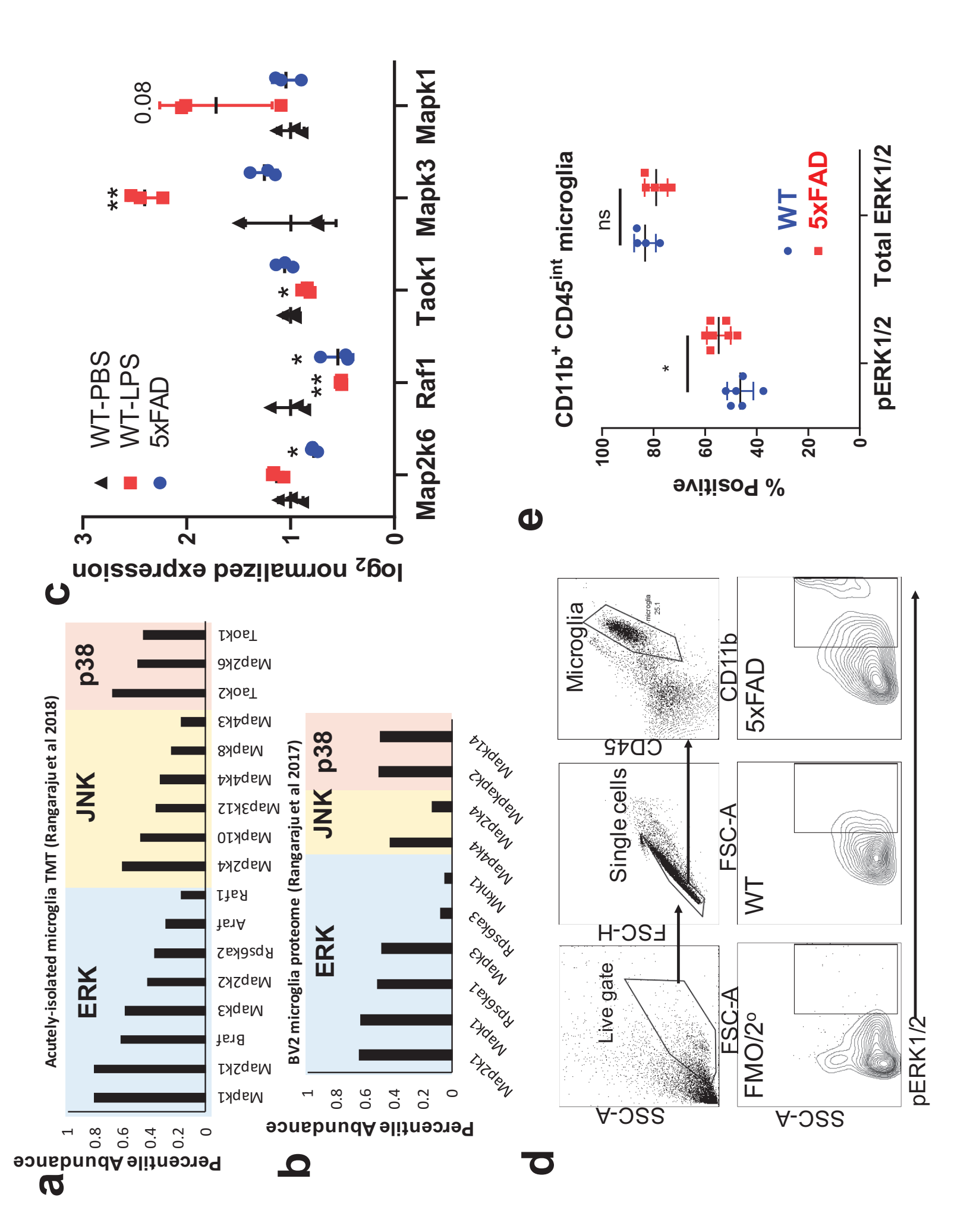
# Figure 7. Phospho-proteomic analysis of human post-mortem brain reveals ERK activation in Alzheimer's disease.

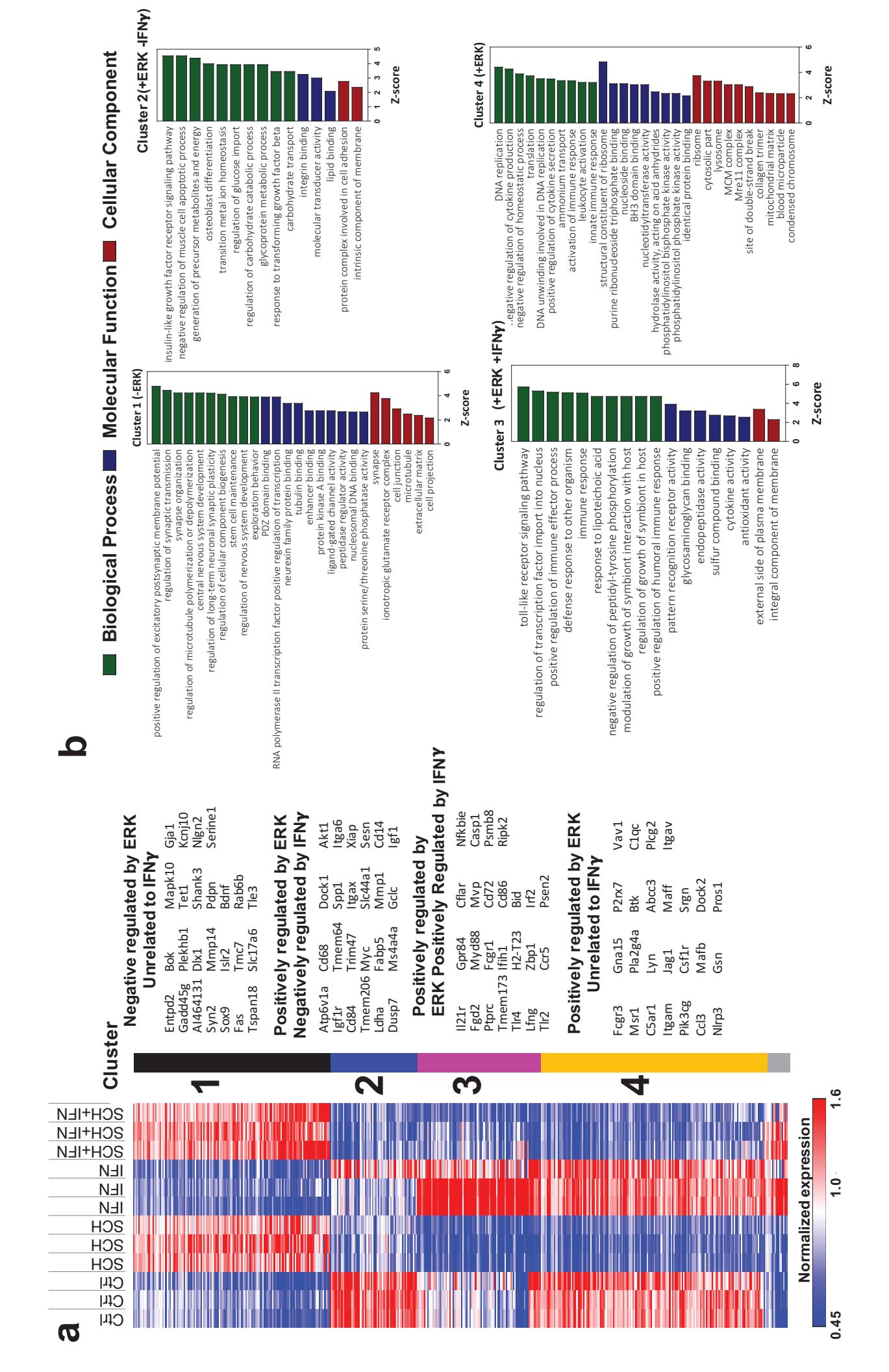
- (a) Heat map showing k-means clustering of 57 differentially expressed phospho-peptides that mapped to a MAPK reference gene list, across frontal cortex samples from six non-Alzheimer's disease control, six asymptomatic Alzheimer's disease, and six symptomatic Alzheimer's disease cases.
- (b) Box and whisker plot quantifying the trajectory of change in expression for each cluster across stages of Alzheimer's disease progression.
- (c) Diagram showing the number of peptides (in parenthesis) and their respective gene symbols (outside of parenthesis) are involved in ERK, JNK, and p38 signaling.

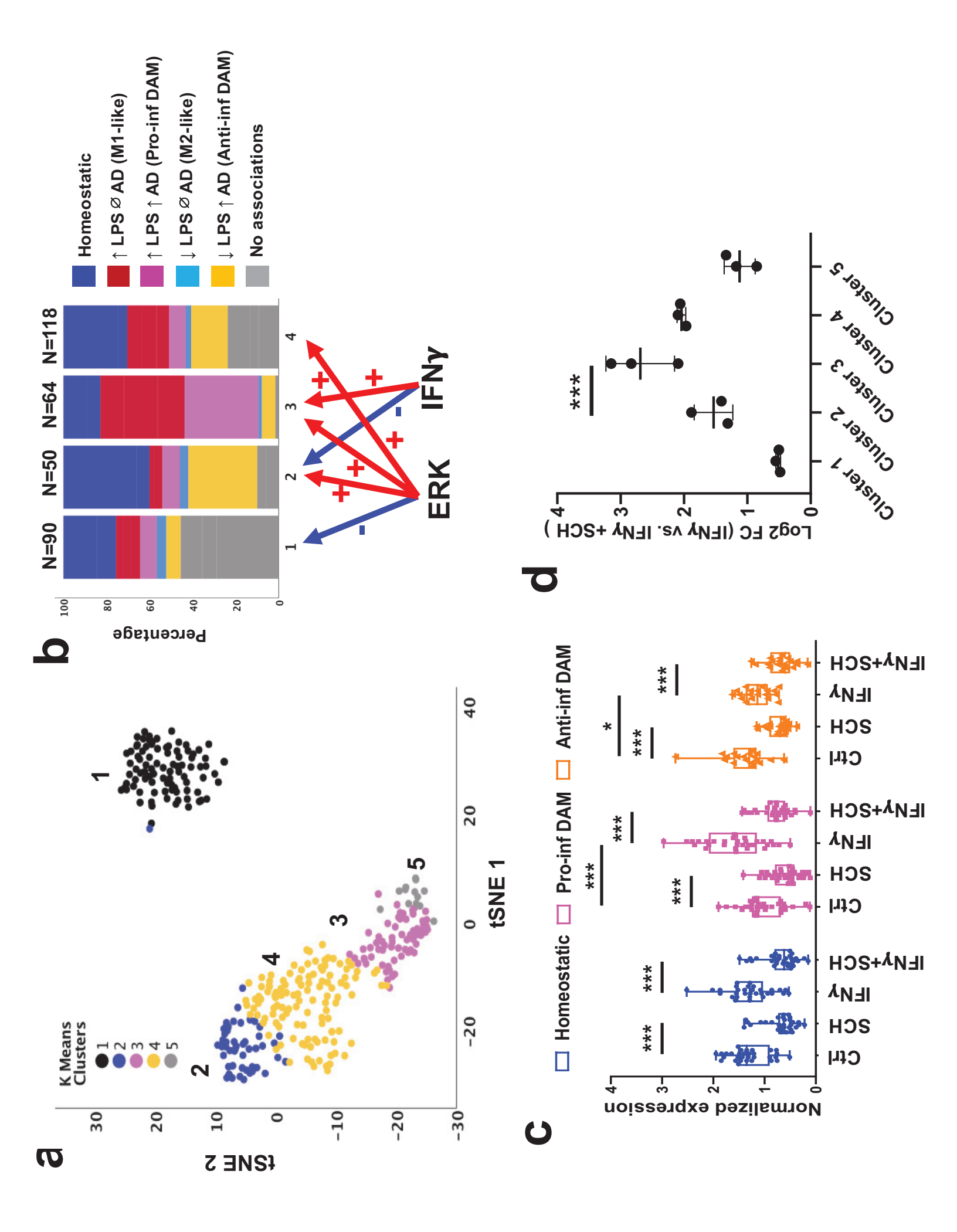
(d) Visual representation and k-means clustering of key phosphosites within the differentially expressed ERK-related peptides in the IMAC dataset, mapping to all levels of the ERK cascade, that are relevant in Alzheimer's disease.

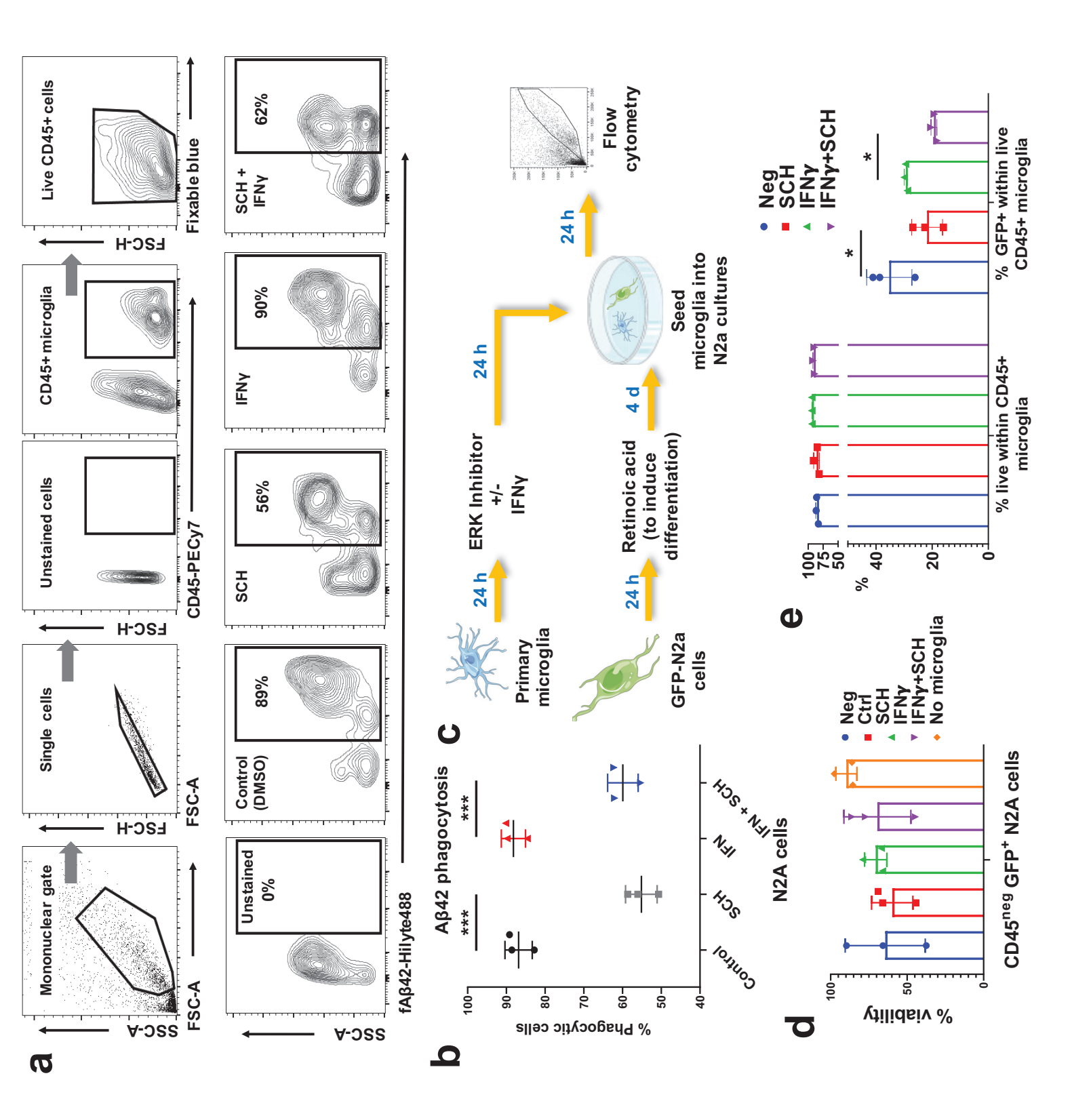
Figure 8. Phospho-proteomics reveals progressively upregulated flux through MAPK pathway in asymptomatic Alzheimer's disease and cognitively-impaired Alzheimer's disease cases. Colored circles represent fold-change of each detected phospho-protein protein compared to control cases (six non-Alzheimer's disease control, six asymptomatic Alzheimer's disease, and six symptomatic Alzheimer's disease cases).

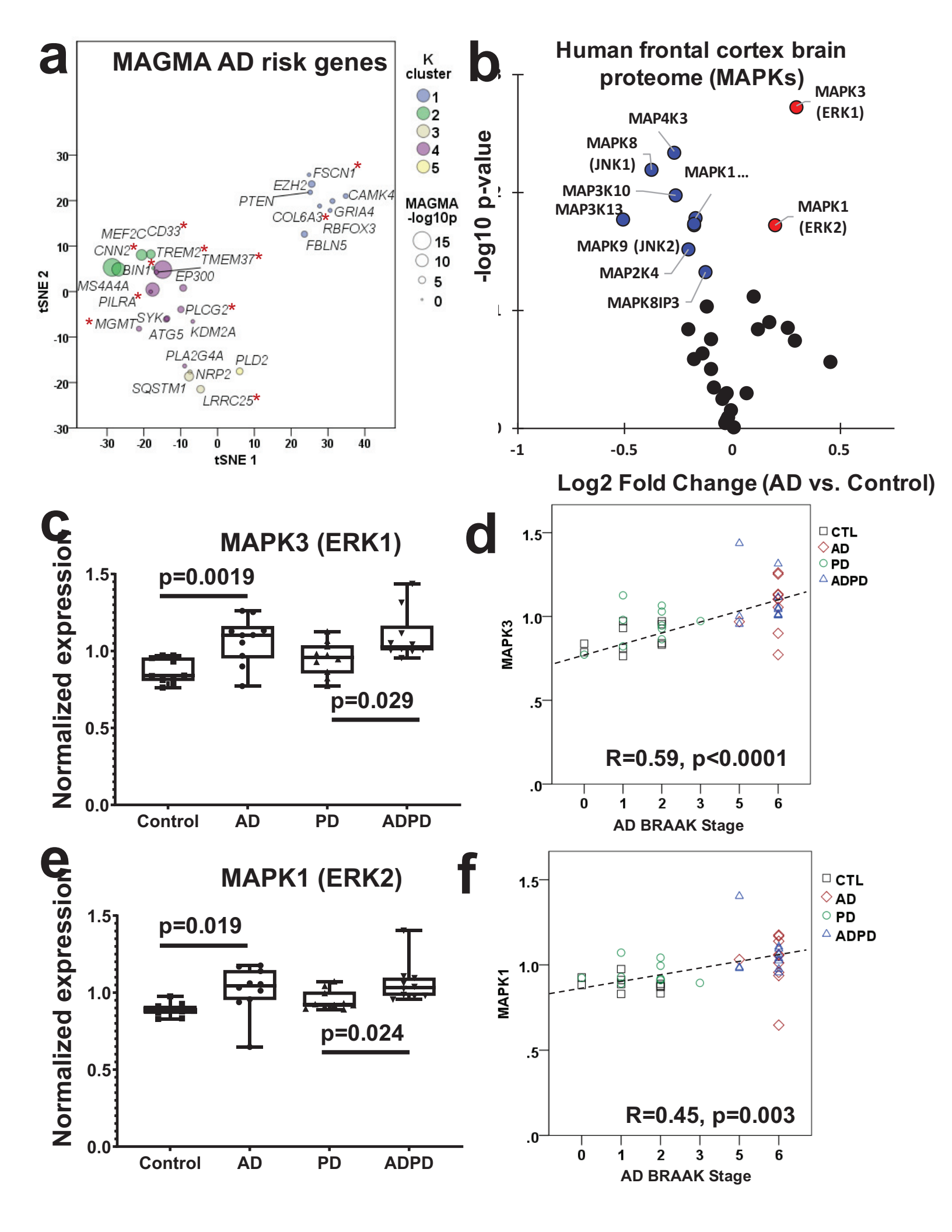


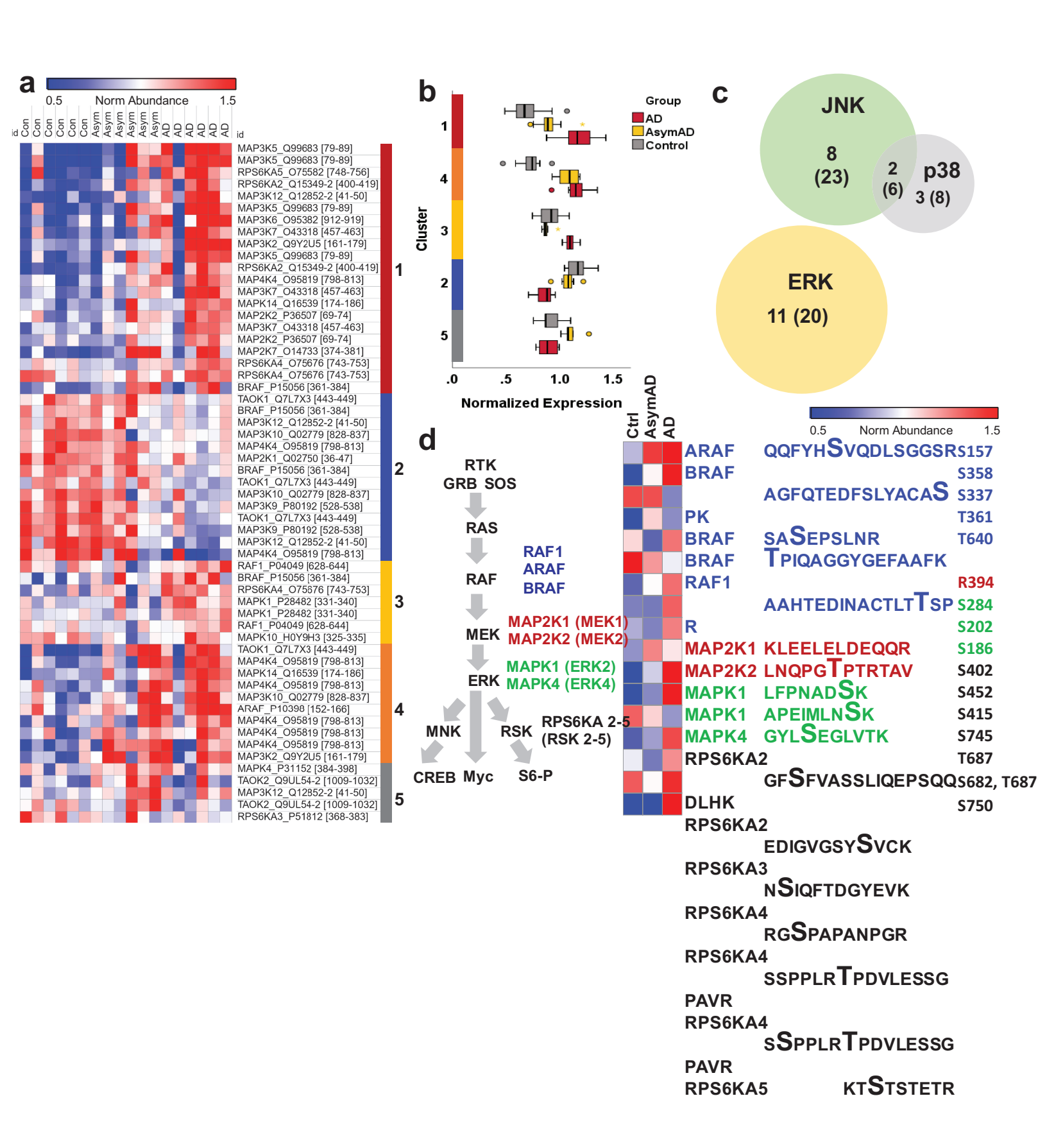


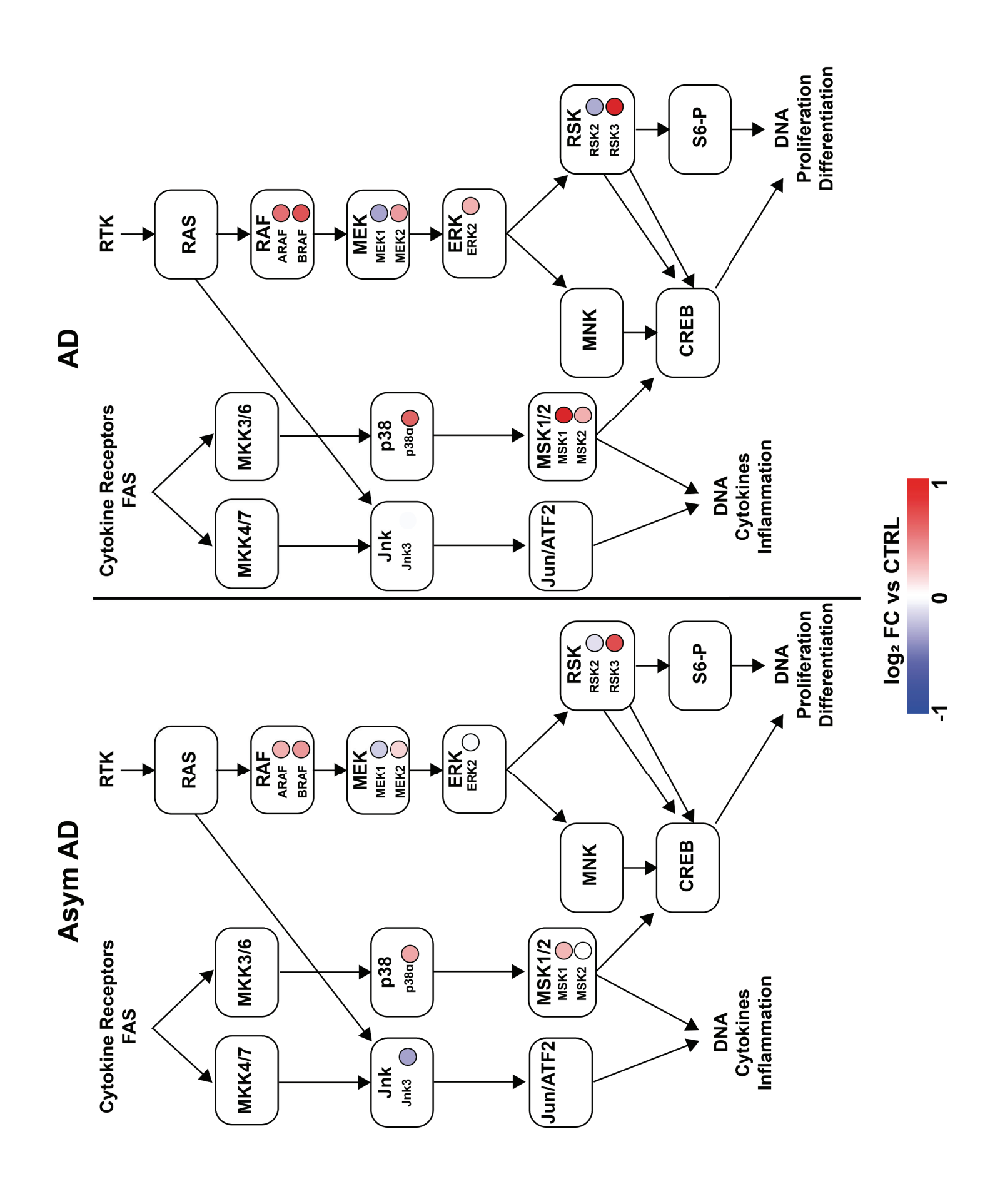












#### SUPPLEMENTAL FIGURES

### ERK regulates microglial immune responses in Alzheimer's disease

#### **Authors**

Michael J Chen,\*1 Supriya Ramesha,\*1 Laura D. Weinstock,<sup>3,4</sup> Tianwen Gao,¹ Linyang Ping,² Hailian Xiao,¹ Eric B Dammer,² Duc D Duong,² Allan I Levey,¹ James J Lah,¹ Nicholas T Seyfried,² Levi B. Wood,\*3,4,5 Srikant Rangaraju\*1

Supplemental figures: 7

<sup>\*</sup>Equal contribution as first authors

<sup>\*</sup>Equal contribution as senior/corresponding authors

<sup>^</sup>Lead contact

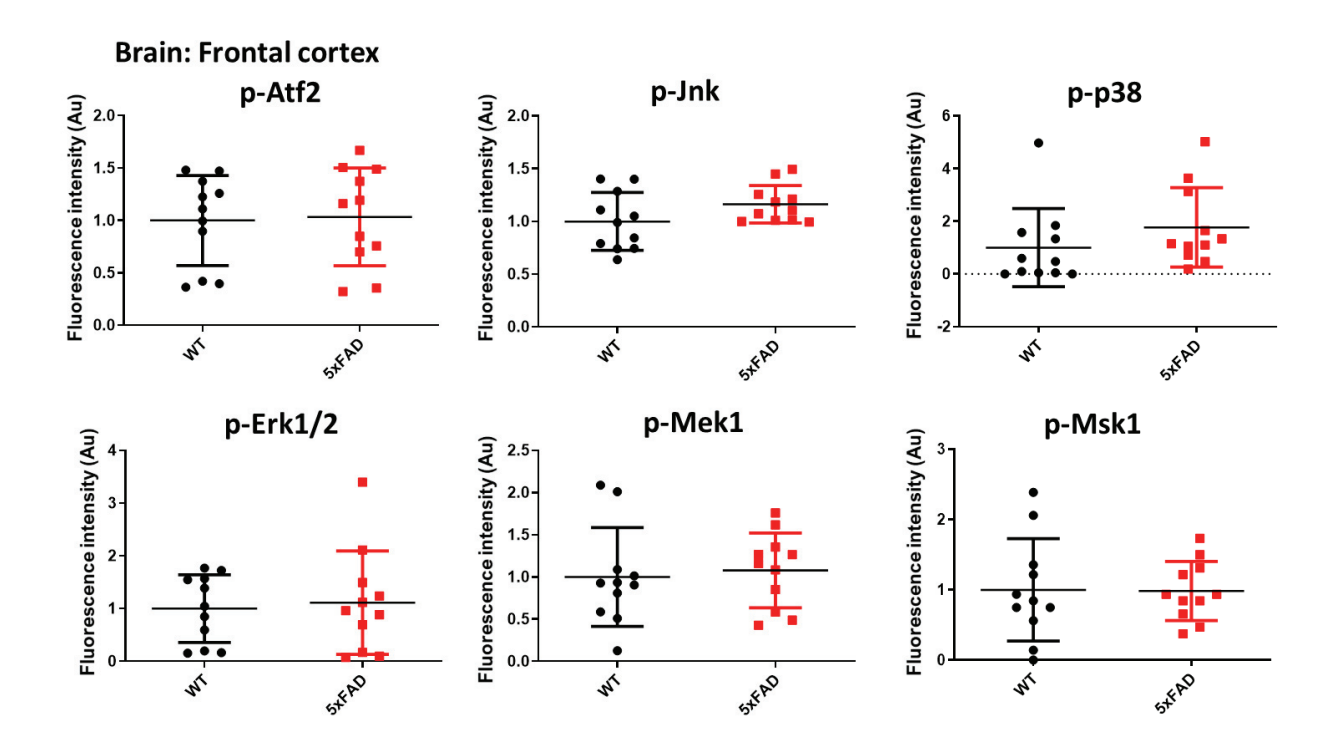
<sup>&</sup>lt;sup>1</sup>Department of Neurology, Emory University, Atlanta GA 30322 USA

<sup>&</sup>lt;sup>2</sup>Department of Biochemistry, Emory University, Atlanta GA 30322 USA

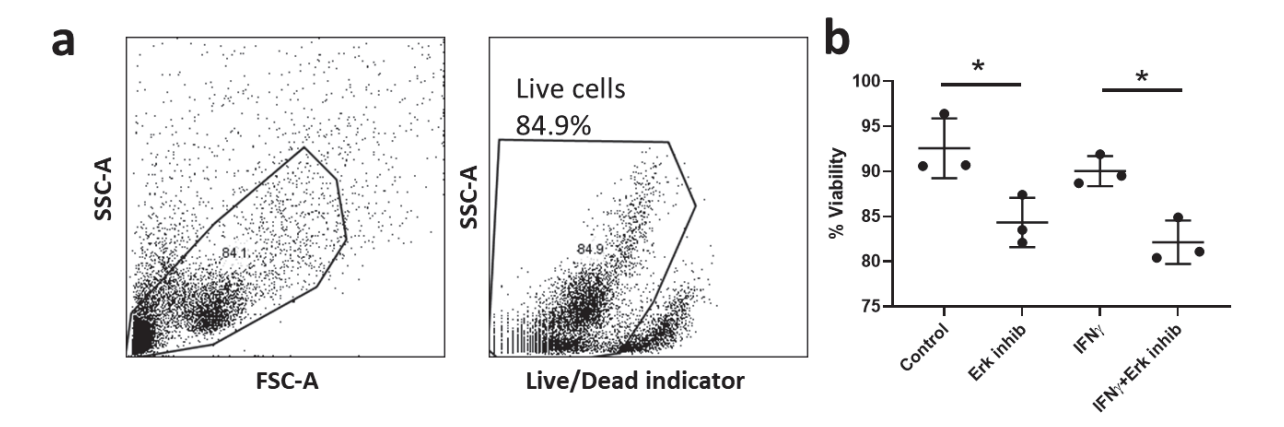
<sup>&</sup>lt;sup>3</sup>Parker H. Petit Institute for Bioengineering & Bioscience, Georgia Institute of Technology, Atlanta, GA 30332

<sup>&</sup>lt;sup>4</sup>The Wallace H. Coulter Department of Biomedical Engineering, Georgia Institute of Technology, Atlanta, GA 30332

<sup>&</sup>lt;sup>5</sup>George W. Woodruff School of Mechanical Engineering, Georgia Institute of Technology, Atlanta, GA 30332

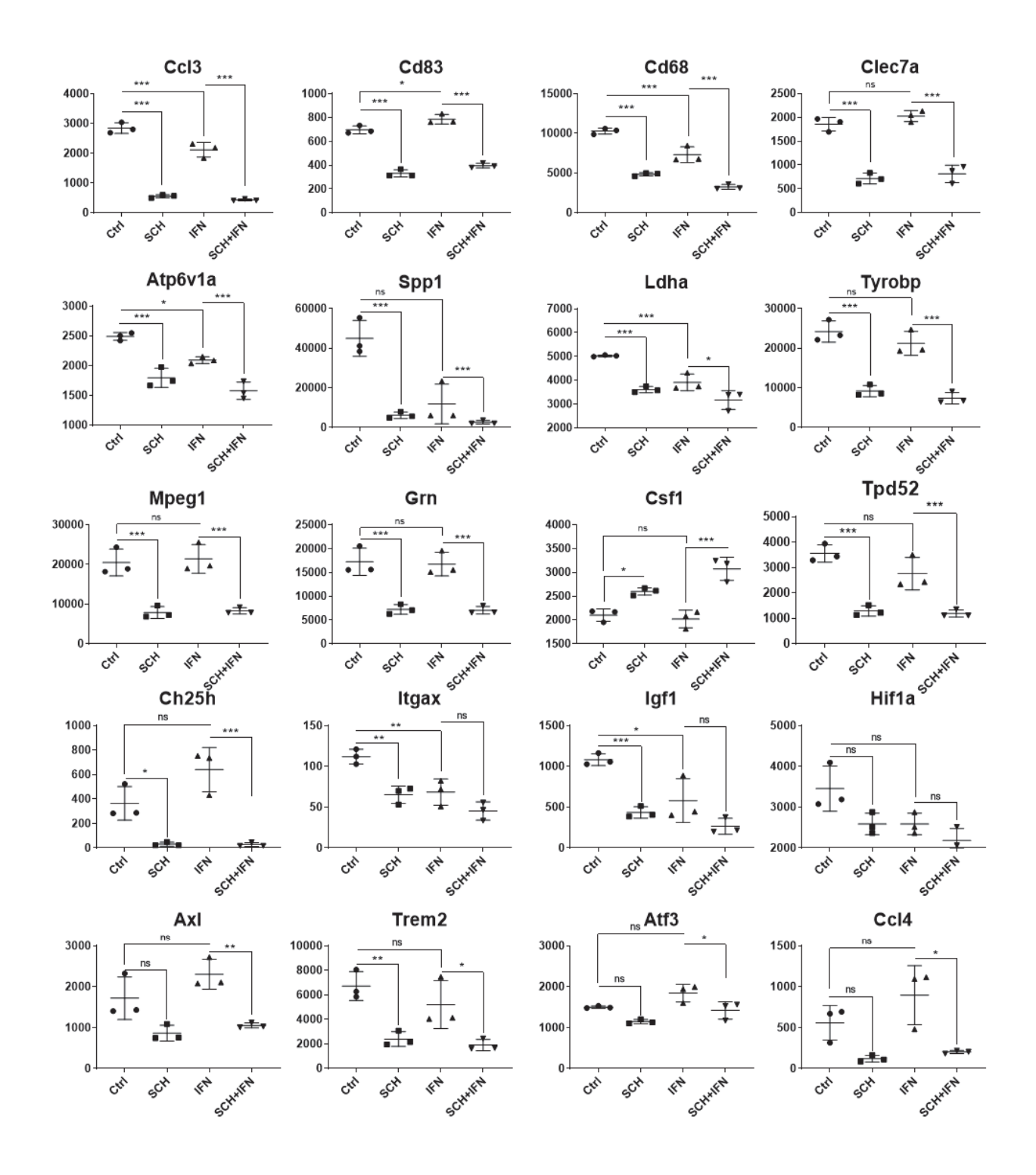


**Supplementary Figure 1.** MAPK phospho-signaling changes in frontal cortex in WT and 5xFAD mouse brain. Mean and SD of the expression of phospho (p)-proteins, as represented by the intensity of fluorescence, are represented.



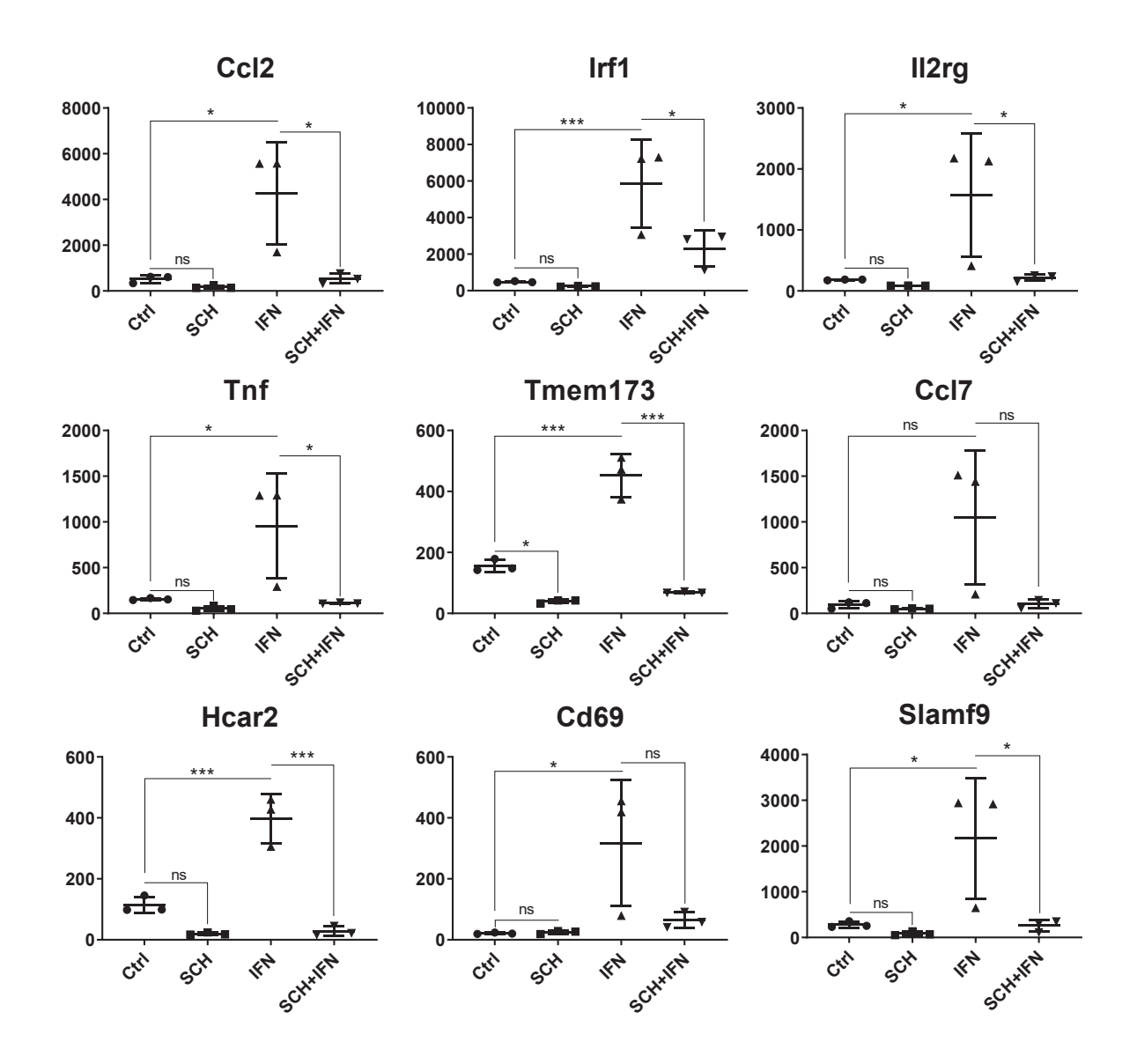
### Supplementary Figure 2. ERK inhibition exerts minimal impact on viability of microglia.

- (a) Flow cytometry gating strategy to identify live cell populations.
- (b) Bar plot showing the slight reduction of viability among ERK inhibited microglia samples. N=3 replicates per group. Error bars represent SD. \*p<0.05

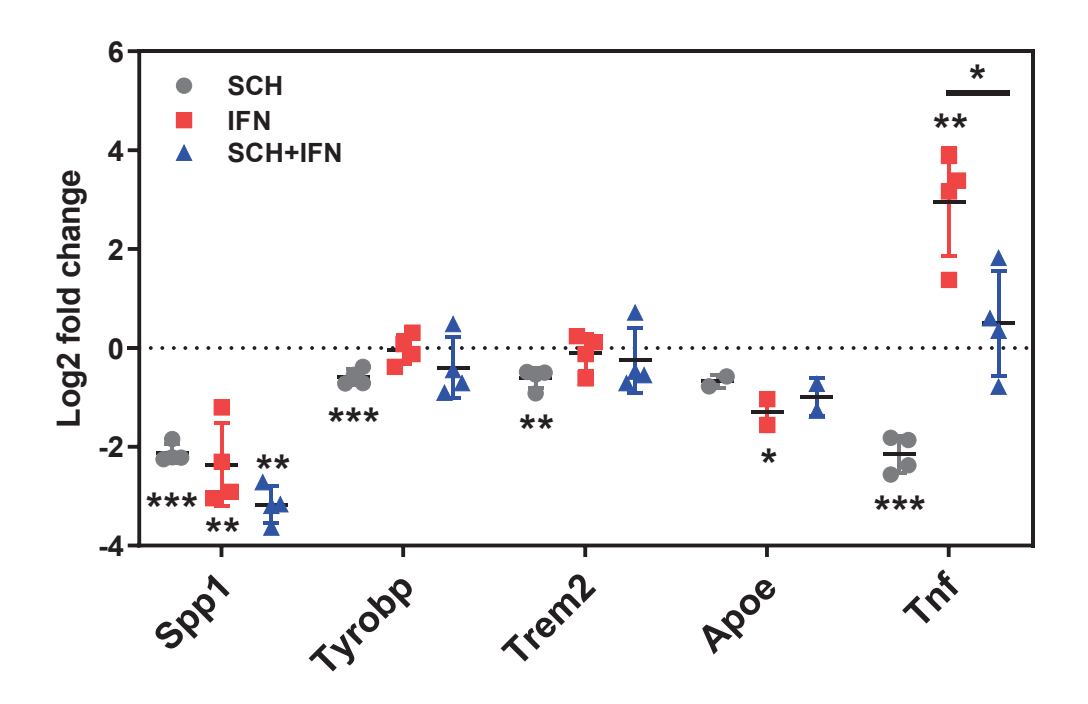


Supplementary Figure 3. DAM genes positively regulated by ERK signaling. Individual NanoString normalized counts data for canonical DAM genes previously identified by single-cell

RNA seq (Keren-Shaul et al, 2017) N=3 replicates per group (Y-axis represents mRNA counts). Error bars represent SD. \*p<0.05, \*\*p<0.01, \*\*\*p<0.005.



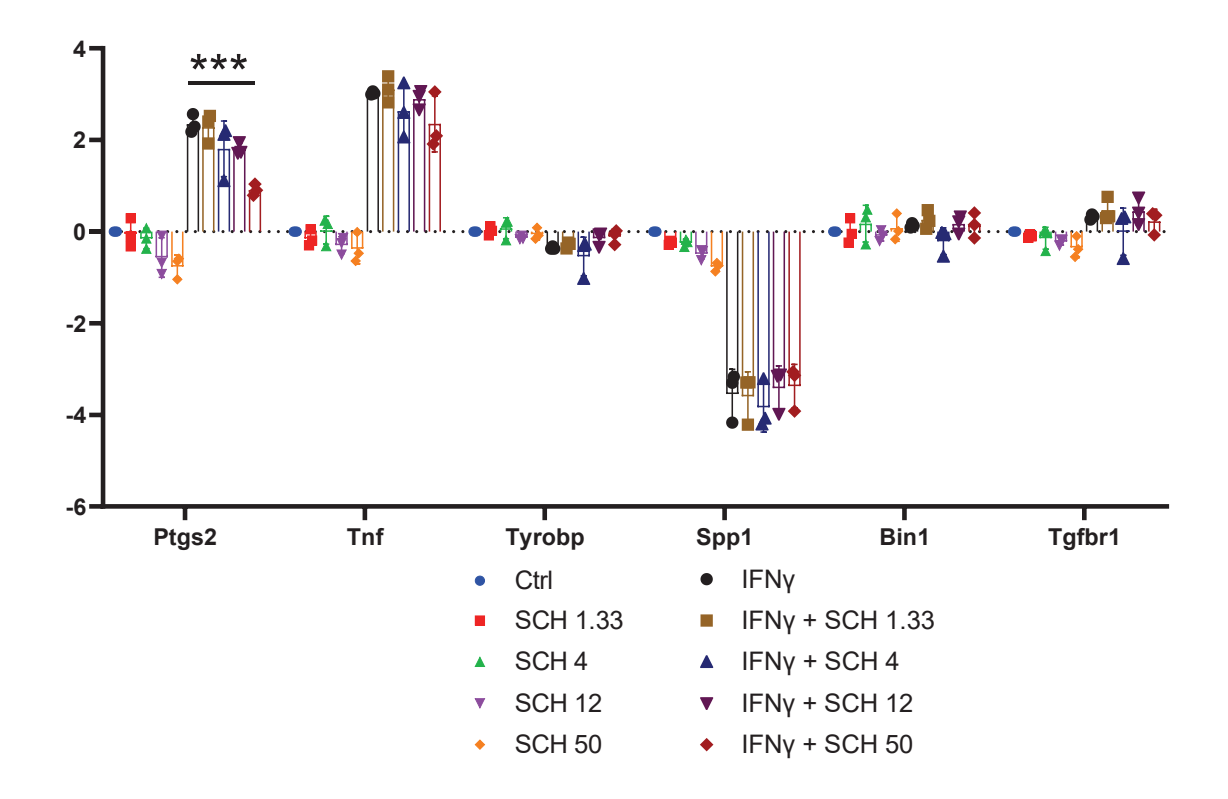
**Supplementary Figure 4. Pro-inflammatory DAM genes positively regulated by ERK signaling.** Individual NanoString normalized counts data for pro-inflammatory DAM genes previously identified by network analyses of microglial transcriptomes (Y-axis represents mRNA counts) (Rangaraju et al, 2018b). N=3 replicates per group. Error bars represent SD. \*p<0.05, \*\*p<0.01, \*\*\*p<0.005.



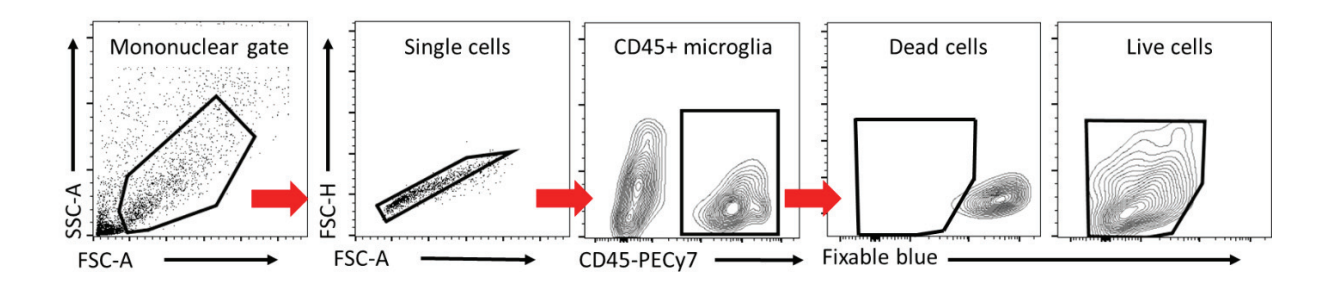
Supplementary Figure 5. qRT-PCR validation confirms ERK effect of select DAM genes.

Relative gene expression normalized to the housekeeping gene GAPDH (2-ΔΔCt method) is

shown. N=3 replicates per group. Error bars represent SD. \*p<0.05, \*\*p<0.01, \*\*\*p<0.005.



**Supplementary Figure 6.** qRT-PCR study showing dose-dependent regulation of proinflammatory DAM but not homeostatic and anti-inflammatory DAM genes by ERK inhibition in primary microglia. Concentrations of the inhibitor (in nM) are given in the figure legend. Relative gene expression normalized to the housekeeping gene GAPDH (2- $\Delta\Delta$ Ct method) is shown. N=3 replicates per group. Error bars represent SD. \*p<0.05, \*\*p<0.01, \*\*\*p<0.005 based Tukey post-hoc pairwise test.



**Supplementary Figure 7.** Flow cytometry gating strategy for live/dead cell distinction. Gating strategy for single brain mononuclear cells expressing CD45 (microglia) is shown. Microglia are further sub-gated to include only live cells using Fixable blue, an amine-based live/dead indicator.